Experimental study on steady-state performance of an axial grooved heat pipe under rotational condition

Yongqi Xie[a], **Kang Sun**[a], **Longzhu Han**[a,*], **Zhen Fang**[a], **Hongwei Wu**[b,**], **Hongxing Zhang**[c]

[a]School of Aeronautic Science and Engineering, Beihang University, Beijing, 100191, China

[b]School of Physics, Engineering and Computer Science, University of Hertfordshire, Hatfield, AL10 9AB, United Kingdom

[c]National Key Laboratory of Spacecraft Thermal Control, Beijing Institude of Spacecraft System Engineering, China Academy of Space Technology, Beijing, 100094, China

[*]Corresponding author. Longzhu Han, Email: hlz@buaa.edu.cn

[**]Corresponding author. Hongwei Wu, Email: h.wu6@herts.ac.uk

Abstract:

This study explores the performance optimization of grooved heat pipes under rotational conditions, focusing on both straight and curved designs. To address the challenges posed by centrifugal forces in rotating systems, we designed and tested a conventional straight grooved heat pipe and a novel curved grooved heat pipe with a variable curvature structure. Experiments were conducted across a range of rotational speeds (0-20 rpm),heat loads (30 W-300 W) and loading methods (heat load before rotation and heat load after rotation) to evaluate the operating performance of both grooved heat pipes. The results indicate that the straight grooved heat pipe struggled to maintain efficiency under rotational conditions, as centrifugal forces caused fluid to accumulate at both ends, leading to higher operating temperatures and reduced heat transfer efficiency. At the case of 20 rpm with a heat load of 110 W, the temperature difference exceeded 25°C, highlighting the limitations of the straight design in such environments. In contrast, the curved grooved heat pipe effectively mitigated the impact of centrifugal forces. Its design reduced liquid accumulation in the condenser section, maintained beneficial acceleration effects in the evaporator section, and improved overall heat transfer performance. Specifically, at 20 rpm, the curved pipe successfully transferred over 300 W with a temperature difference not exceeding 5°C, demonstrating its superior performance. However, at higher rotational speeds and lower power levels, the curved design also showed some limitations, as excessive fluid accumulation in the evaporator section led to a shift in the evaporation site, increased thermal resistance, and a certain degree of superheating. These findings highlight the potential of the variable curvature design in improving the efficiency of grooved heat pipes under rotational conditions. This work advances the understanding of fluid dynamics and heat transfer mechanisms in such systems, offering insights that could inform the design of more efficient heat pipes for rotating applications.

Keywords: Satellite Cooling; Grooved Heat Pipe; Structural Design; Operational behavior; Rotating Environments;

Nomenclature

I	Current of heat load supply	[A]
L	Length	[m]
m	Mass	[kg]
Δp	Pressure difference	[Pa]
Q	Heat load	[W]
R	Thermal resistance	[K/W]
T	Temperature	[K]
U	Voltage of heat load supply	[V]
w	Rotational angular velocity	[°/s]
x	Independent vary	
y	Physical quantity	

Subscripts

c	Condenser
e	Evaporator
fc	Flow Component
max	Maximum
min	Minimum

Acronyms

AGHP	Axial grooved heat pipes
DC	Direct Current
GHP	Grooved heat pipes
PT100	Platinum Resistance Thermometer (100 ohms)

1. Introduction

Spin-stabilized satellites maintain stability through rapid rotation, leveraging the conservation of angular momentum [1-3]. This approach ensures stable orientation and trajectory [4-6]. The rotational velocity can vary significantly based on mission and design requirements, typically ranging from a few to several hundred revolutions per minute [7-9]. These rotational loads present cooling challenges for the satellite. Currently, passive cooling methods such as heat sinks, multi-layer insulation, and surface coatings are used [10-15]. However, these methods have limited regulatory capabilities [16-18] and can lead to uneven temperature distribution under periodic thermal load changes [19-21]. Consequently, new thermal control methods are needed for rotating environments. Grooved heat pipes (GHPs) are efficient heat transfer components that offer strong heat conduction [22-23], small operating temperature differences [24-25], and uniform surface temperature control [26-27]. These advantages have led to their widespread application in spacecraft thermal control [28-32].

Recently, GHPs have become a central focus of research, particularly in optimizing their performance for high heat flux densities. Current studies primarily aim to improve the evaporation-condensation processes, enhance capillary structures, and investigate the effects of gravity on performance. In optimizing the evaporation and condensation processes in heat pipes, Zhang et al.[33] combined experimental and numerical simulation methods to regulate these processes using the latent heat of phase change materials. This approach resulted in a 27.4% reduction in the maximum temperature of the evaporator section. Liu et al.[34] examined the impact of different length ratios between the evaporator and condenser sections on the thermal performance of aluminum flat heat pipes, finding that a length ratio of 1.0 maximized heat transfer performance. Lv et al.[35] proposed a silicon-based ultrathin flat grooved heat pipe with dual-end cooling and used visualization techniques to study its evaporation mode under various heat loads and tilt angles. Their results indicated that axial GHPs exhibited a unique corner film evaporation mode due to the combined effects of gravity and capillary forces. Tang et al.[36] introduced a novel cooling method by heating both ends of the heat pipe and placing a condenser in the middle, addressing the cooling challenges of multi-heat source systems in horizontal or inclined orientations. Their experimental results showed that this method offered high thermal performance, low cost, and operational simplicity. Anand et al.[37] experimentally studied the effect of evaporator length on the heat transfer of axial grooved ammonia heat pipes. Their findings revealed that as the evaporator length increased, the maximum heat transfer capacity increased by 1.6 to 2.5 times the original capacity.

In the field of capillary enhancement, Saygan et al.[38] employed techniques such as grooved bifurcation and gradient wettability surfaces, significantly reducing thermal resistance and proposing a predictive model for liquid flow velocity within the grooves. Ving et al.[39] and Chang et al.[40] enhanced the thermal conductivity of heat pipes by coating their inner surfaces with graphene nanostructures and nickel-graphene nanocomposite coatings, respectively, increasing the thermal conductivity by 3 times and 7 times the original values. Cheng et al.[41] constructed gradient wettability surfaces, which could reduce the thermal resistance of grooved copper heat pipes by up to 92.6%, while a negative wettability gradient

would lead to insufficient working fluid return. Mohammad Hamidnia et al.[42] designed and fabricated micro-columns of different shapes within microgrooves to improve flow boiling heat transfer, finding that circular and sawtooth micro-columns outperformed other shapes. Li et al.[43] compared the thermal performance of three different composite wick structures in heat pipes, revealing that single-arc sintered groove wicks had the lowest evaporative thermal resistance, while mesh groove wicks exhibited the lowest condensation thermal resistance.

The impact of gravity on thermal performance has been widely studied. Parand et al.[44] demonstrated that under zero-gravity conditions, different working fluids significantly influence the thermal performance of heat pipes. Sudhan et al.[45] improved the heat transfer performance of GHPs under both gravity and anti-gravity conditions by using an oxide layer on copper, finding that the maximum heat transfer capacity of narrow grooves was seven times that of wide grooves under anti-gravity conditions. Zhang et al.[46] investigated the effect of inclination angle on the performance of axial trapezoidal GHPs and found that as the inclination angle increased, the thermal resistance decreased and the heat transfer coefficient increased. Tang et al.[47] developed an axial graded wick structure to enhance the heat transfer performance of cylindrical heat pipes in the anti-gravity direction, showing that the maximum heat transfer capacity of the axial gradient heat pipe at a 90° inclination was 75% higher than that of the uniform wick heat pipe. Jacob et al.[48] studied the heat transfer performance of flat GHPs with different working fluids at various inclination angles, finding that a special working fluid reduced thermal resistance by about 20%, nearly tripled the capillary limit, and increased the maximum operational inclination angle. Yu et al.[49] experimentally examined the evaporation mode of heat pipes at small inclination angles, revealing that liquid film evaporation gradually became dominant at small inclination angles.

Regarding the impact of acceleration on the operating performance of heat pipes, Voigt et al.[50] studied the effect of different translational accelerations on heat pipe performance and found that as translational acceleration increased, the heat transfer limit of the heat pipe decreased to less than half of its original value. However, there have been no reported studies on the application and performance improvement of GHPs in rotational scenarios. Xie et al.[51] conducted a visualization study on loop heat pipes in rotational environments, observing phenomena such as liquid surface inclination in the liquid transport lines and film condensation becoming the dominant mechanism in the condenser due to rotational angular velocity. Their results indicated that rotational angular velocity affects the evaporation and condensation processes of loop heat pipes to varying degrees.

Research on the operating characteristics of axial grooved heat pipes (AGHPs) has primarily focused on micro-gravity and gravity fields, with little exploration of internal flow and heat transfer mechanisms under rotational conditions. The complexities introduced by centrifugal forces, particularly the impact on fluid return and overall heat transfer efficiency, have not been sufficiently addressed in the literature. Detailed experimental data and mechanistic analyses concerning the performance of AGHPs under varying rotational speeds are notably lacking, especially in terms of the effects on heat transfer limits and thermal resistance. To address this gap, the present study proposes a novel approach that employs a variable curvature design to leverage centrifugal forces during rotation, thereby enhancing fluid return and mitigating

adverse effects. Two sets of Ω-shaped aluminum-ammonia grooved heat pipes with distinct geometries were designed and fabricated. One set featured a curved design specifically intended to optimize performance. Experiments conducted across different rotational speeds, heat loads, and loading methods were used to explore the effects of these variables on the steady-state performance of grooved heat pipes in rotational environments, alongside an analysis of the internal flow and heat transfer mechanisms.

2. Experimental apparatus and conditions

2.1 Experimental setup

The experimental system is illustrated in Fig. 1. The test rig mainly consists of an acceleration simulation system, a fixture system (including test pieces), a heating system, a cooling system, and a data acquisition system. During the experiment, the rotational velocity of the system can be manually adjusted. The heat load is regulated by varying the output current, the heat sink temperature is controlled by setting the temperature of a thermostatic water bath, and the temperature of the outer sidewall of the heat pipe is measured using a data acquisition instrument (Agilent 34970A).

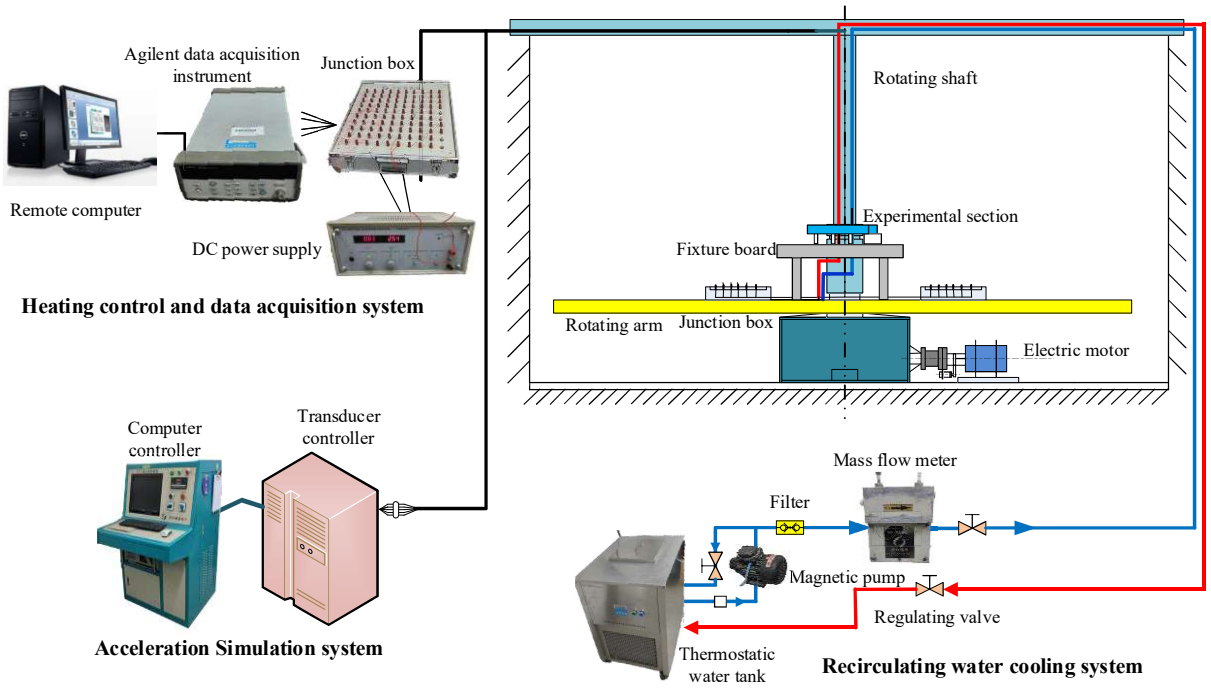

Fig. 1. The Schematic of the AGHP Testing Experimental System.

The acceleration simulation is conducted using the constant acceleration simulation centrifuge, as shown in Fig. 2. This centrifuge can be controlled either by a dedicated desktop computer program or manually. For this experiment, manual control was chosen to achieve precise control of low rotational velocities during the test. The centrifuge is equipped with a junction box that transmits electrical signals and temperature sensor signals during rotation.

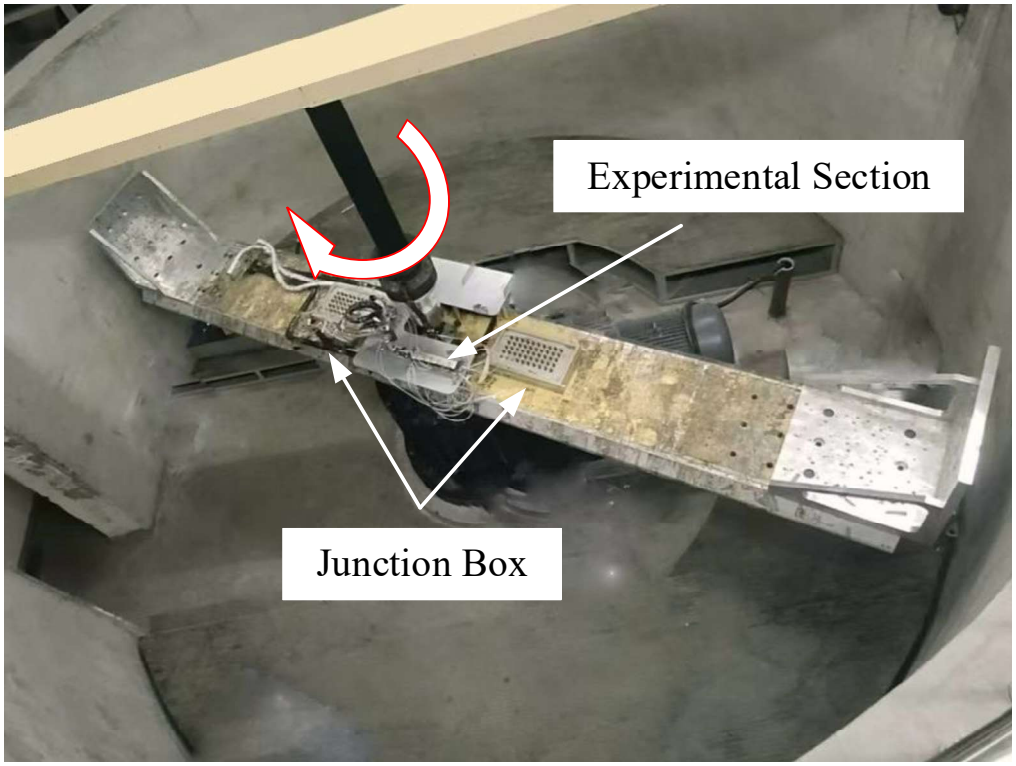

Fig. 2. Photograph of the Constant Acceleration Simulation Centrifuge.

To closely simulate practical application scenarios, the fixture was arranged near the rotational axis, as shown in Fig. 3. First, the fixture board was secured to the support column, and the heat pipe was fixed to the positioning/insulation block with pre-set threaded holes using bolts and clamps. To eliminate the influence of gravity, the levelness of the heat pipe was measured during both installation and experimentation, ensuring it remained horizontal. A DC power supply was used to heat the 40-ohm resistive heating film attached to the upper surface of the evaporator section. The power supply featured a current measurement accuracy of 0.5% and a voltage measurement accuracy of 0.1%. The heat was then transferred through the AGHP and cooled at the condenser end by circulating low-temperature water. The cold plate used in this experiment is shown in Fig. 3. It contains microchannels to enhance heat transfer. Thermal grease was applied between the cold plates and the condenser end of the AGHP to reduce contact thermal resistance. The temperatures recorded during the experiment were measured using calibrated PT100 platinum resistance thermometers, with an accuracy of ±0.3°C. Temperature measurement points were positioned on the outer sidewall of the heat pipe according to GB/T 14812-2008 standards. Following installation, insulation material was wrapped around the experimental setup to minimize heat exchange with the environment.

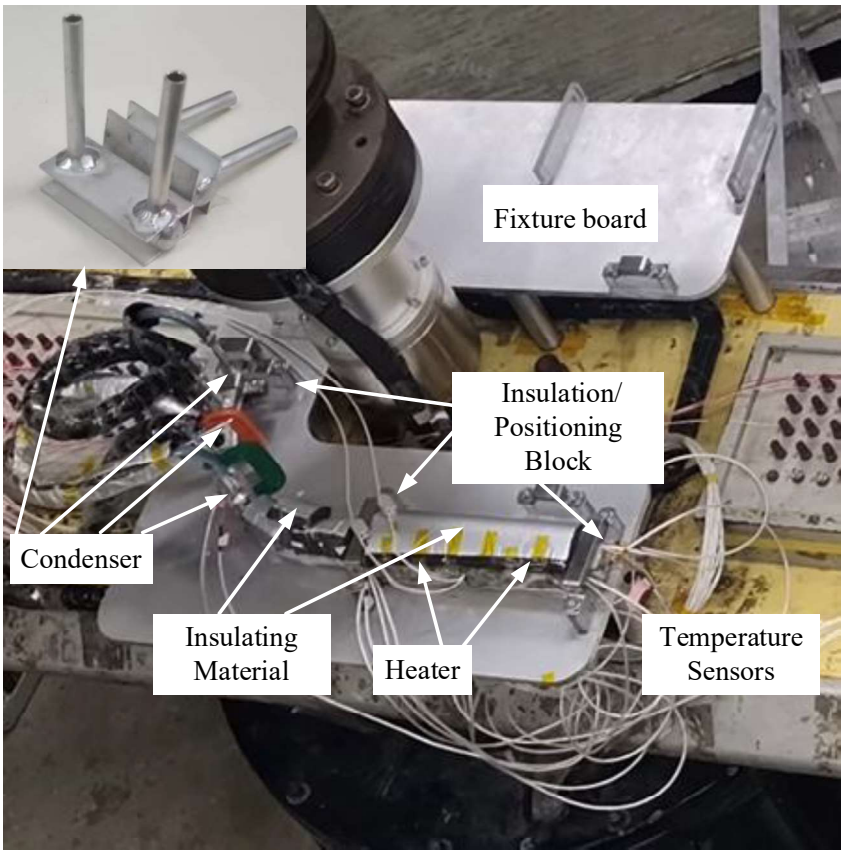

Fig. 3. AGHP Test Apparatus Setup.

2.2 Specifications of AGHPs

In this study, two sets of aluminum-ammonia AGHPs were fabricated, with specific parameters detailed in Table 1. Fig. 4 presents the external designs of the two heat pipes. The heat pipes feature Ω-shaped grooves, with a total of 14 grooves. During the experiment, heating and cooling were applied to the top surface of the heat pipes, with temperature sensors attached to the side walls.

The straight grooved heat pipe (AGHP1#) has a total length of 420 mm, with an evaporator section measuring 140 mm. The condenser section has two experimental configurations: 70 mm and 140 mm, corresponding to adiabatic sections of 210 mm and 140 mm, respectively. The external shape is shown in Fig. 4(a).

The curved grooved heat pipe (AGHP2#) features an optimized design with variable curvature. It starts with a straight section of 300 mm from the evaporator end and a straight section of 75 mm from the condenser end, with a curved section in between for the transition. The radius of curvature gradually decreases from 180 mm to 160 mm (from the evaporator end to the condenser end). It has a total length of approximately 700 mm, with both the evaporator and condenser sections measuring 280 mm, and the adiabatic section approximately 140 mm. The external shape is illustrated in Fig. 4(b).

Table 1 Primary parameters of the AGHPs.

Components	Material	Parameter	Dimensions
		Length/width/height (mm)	420/30/15
		Filling quality (g)	25(100%)
AGHP1#	Aluminum	Evaporation section length (mm)	140
		Insulation section length (mm)	210/140
		Condensation section length (mm)	70/140
		Length/width/height (mm)	700/30/15
		Filling quality (g)	42(100%)
AGHP2#	Aluminum	Evaporation section length (mm)	280
		Insulation section length (mm)	140
		Condensation section length (mm)	280
Working fluid	Ammonia		

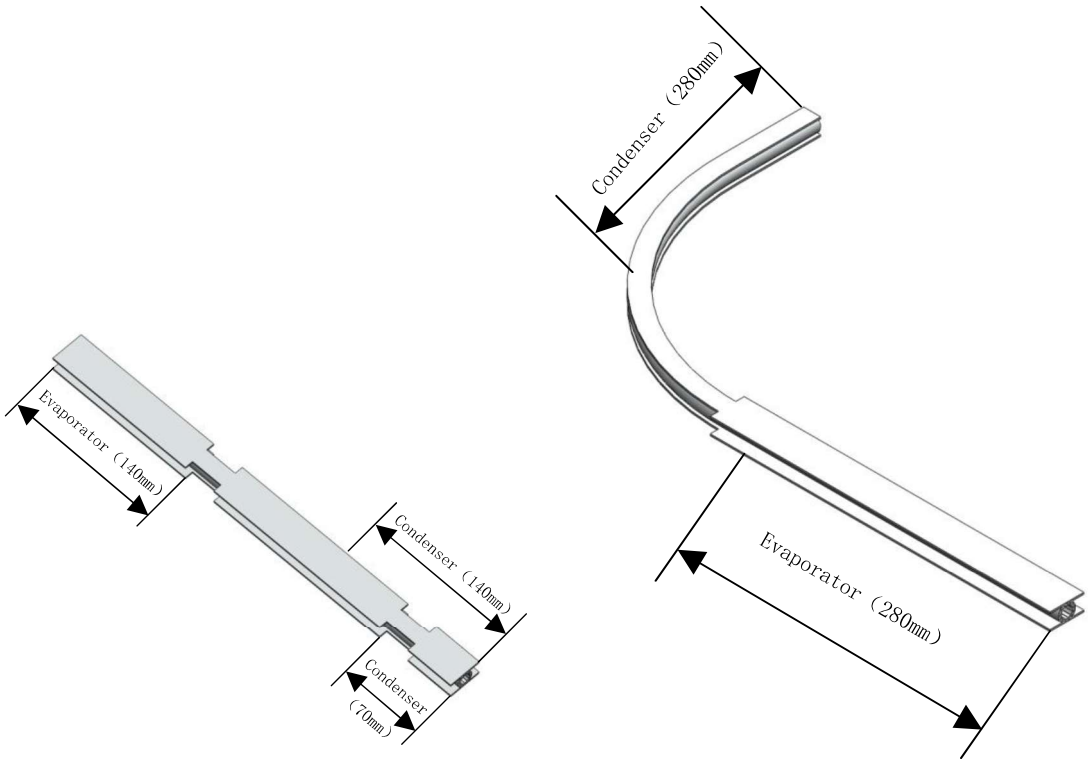

(a) The straight grooved heat pipe (AGHP1#) (b) The curved grooved heat pipe (AGHP2#)

Fig. 4. Shape of the AGHPs.

2.3 Experimental conditions

The experimental conditions for this study are detailed in Table 2, including the static state and four different rotational angular velocities, along with two different shapes (straight and curved). The temperature distribution under load and the maximum heat transfer capacity are crucial indicators for evaluating heat pipe performance. Therefore, the study focused on testing the operating temperature and heat transfer limits of the grooved heat pipes. The heat transfer limit was defined as the power level where the temperature difference between the highest point of the evaporator section and the lowest temperature of the condenser section reached 5°C. Temperature distribution data were analyzed to calculate the thermal resistance of the heat pipes. Finally, the experimental data of different shapes were compared to analyze the impact of shape structure on the steady-state operating performance of the heat pipes. Fig. 5 shows the relationship between the heat pipes and the rotational center under experimental conditions, including the specific positions of measurement points arranged on the outer sidewall.

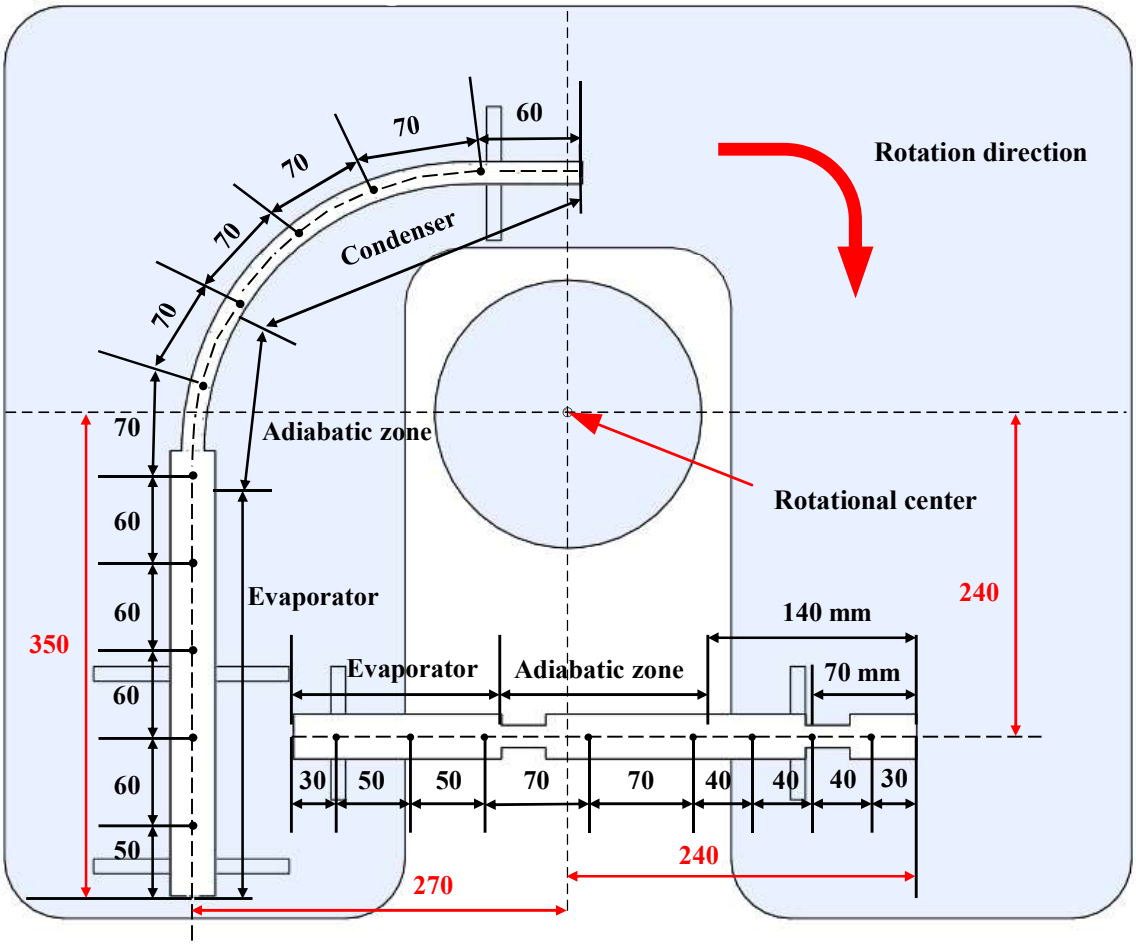

Fig. 5. Position to the Rotational Center and Measurement Points(units: mm)

Table 2 Experimental conditions.

Parameter	Variation
Angular Velocity(rpm)	0, 6, 8, 12, 20
Loading Methods	A(AGHP1#) , A and B(AGHP2#)
Heat load (W)	30 W - 150 W（AGHP1#）
	30 W - 300 W（AGHP2#）
Condenser Length	70 mm and 140 mm（AGHP1#）
	140 mm（AGHP2#）

The temperature distribution was tested after achieving thermal equilibrium and then applying various rotational angular velocities until stability was achieved. In addition to the static state, rotational angular velocities of 6 rpm, 8 rpm, 12 rpm, and 20 rpm were selected.

The heat load levels of the AGHP1# were set at 30 W, 50 W, 70 W, 90 W, 110 W, 130 W, and 150 W. The condenser length was tested in two configurations: 70 mm and 140 mm.

The heat load levels of the AGHP2# were set at 30 W, 50 W, 70 W, 90 W, 110 W, 130 W, 150 W, 170 W, 190 W, 210 W, 230 W, 250 W, 275 W, and 300 W. To account for potential steady-state operational differences due to different loading methods [52], two different loading methods (named A and B) were employed. In method A, heat load was applied first until thermal equilibrium was reached, followed by the application of rotational angular velocity. In method B, rotational angular velocity was applied first until the temperature distribution stabilized, followed by the application of heat load.

2.4 Data uncertainty

For a given physical quantity y, which is a function of independent variables (x_1, x_2, …, x_n), the uncertainty in y can be calculated using the Eq. (1) [53].

$$\frac{\delta y}{y} == \left[\sum_{i=1}^{n} \left(\frac{\partial y}{\partial x_i} \frac{\delta x_i}{y} \right)^2 \right]^{1/2} \tag{1}$$

where δy represents the measurement error of y, and δx_i denotes the maximum measurement error of the independent variable x_i.

In this study, thermal resistance R is a crucial parameter representing the operational performance of the AGHPs and can be calculated by Eq. (2).

$$R = \frac{T_{e,max} - T_{c,min}}{Q} \tag{2}$$

The uncertainty in this experiment primarily arises from the data acquisition and heating control system. The PT100 temperature sensor has an accuracy of approximately ±0.3°C. Taking into account the influence of the data logger, electric wires, junction terminals, slip rings, and the temperature sensor, the maximum temperature measurement uncertainty is 2.53%. The heat load is determined as the product of voltage and current, with maximum uncertainties of 0.81% for voltage and 2.02% for current. Therefore, the maximum uncertainty in the heat load is 2.16%. Based on the above considerations, the uncertainty in the thermal resistance is calculated to be 3.32%.

3. Results and discussion

3.1. Steady-state operating characteristics of straight grooved heat pipes (AGHP1#)

As shown in Fig. 6, a perpendicular line is drawn from the rotational center to the heat pipe, serving as the polar axis in a polar coordinate system. The acceleration component along the flow direction of the working fluid can be derived by Eq. (3). As the position of the working fluid approaches the ends, the distance increases, causing a corresponding increase in the acceleration component.

$$a_{fc} = \omega^2 r \sin\theta = \omega^2 d \tag{3}$$

where r is the radial distance, θ is the polar angle, and d is the distance from the perpendicular foot to the measurement point.

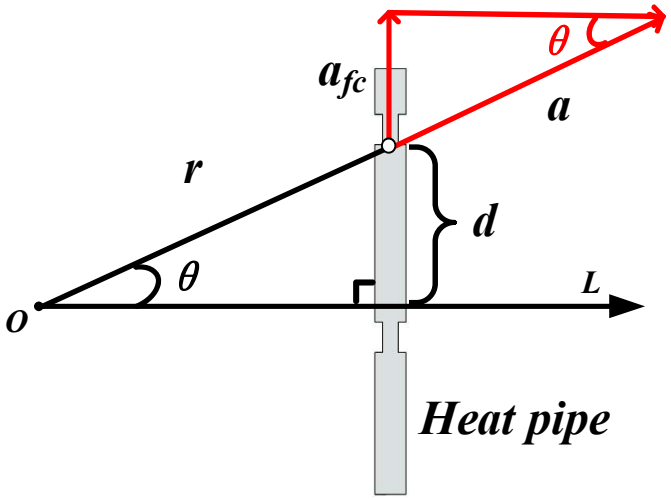

Fig. 6. Polar Coordinate Diagram of Acceleration Analysis.

Fig. 7 presents the variation of the acceleration components in the flow direction at different positions along the straight grooved heat pipe under rotational conditions. The acceleration

component that promotes liquid flow from the condenser section to the evaporator section is defined as positive. It can be observed that the closer to the ends, the greater the magnitude of the acceleration. The acceleration in the evaporator section aids in the return flow of the liquid, while the acceleration in the condenser section hinders the return flow, causing liquid accumulation in the condenser section. This accumulation reduces the effective condensation length and the heat transfer distance.

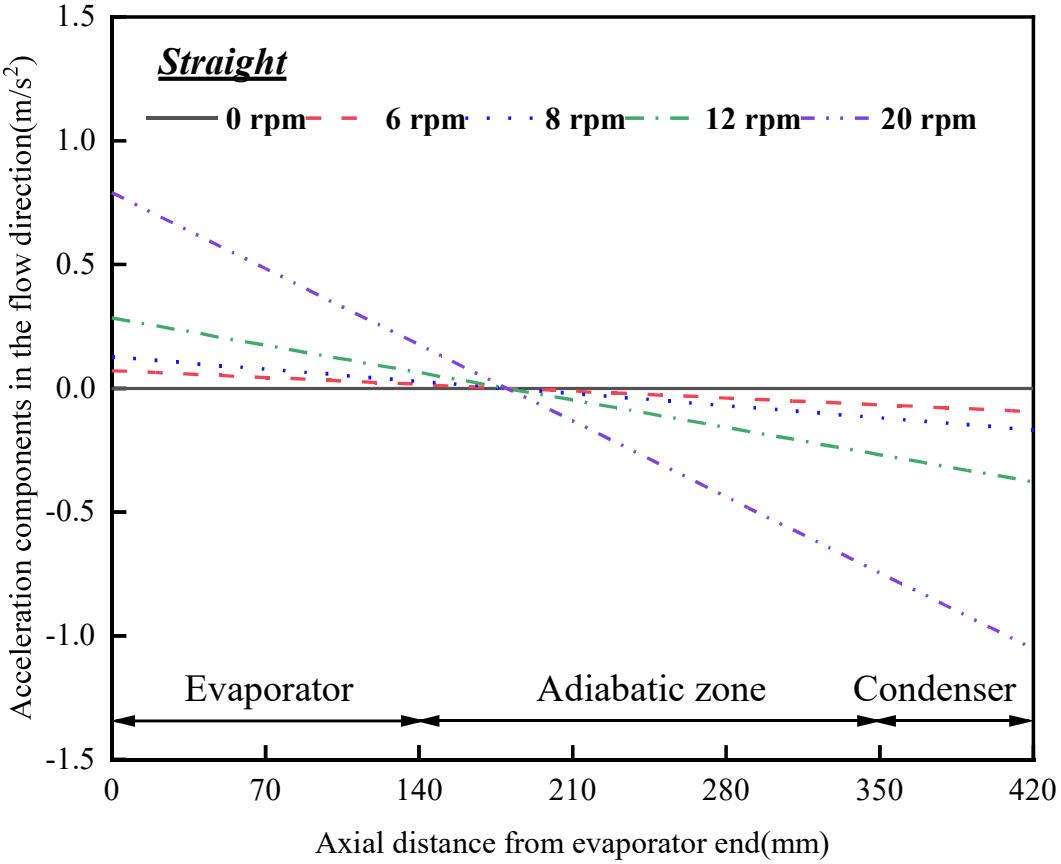

Fig. 7. Acceleration components in the flow direction of the straight grooved heat pipe

3.1.1. Effect of different rotational angular velocity

Fig. 8 illustrates the temperature variations at each measurement point for the straight grooved heat pipe with 70mm condensation length under different rotational velocities and two different heat loads of 30 W and 110 W. As the rotational velocity increases to 20 rpm, there is a significant change in the overall operating temperature of the heat pipe compared to other conditions. The temperature at the end of the condenser section drops considerably, approaching the heat sink temperature, while the temperatures of the evaporator and adiabatic sections rise markedly.

In Fig. 8(a), at a heat load of 30 W, the maximum temperature in the evaporator section

remains around 22.5°C, while the minimum temperature in the condenser section is around 21.5°C at rotational velocities of 0-12 rpm. The temperature values at the same position show slight differences, with a maximum operating temperature difference not exceeding 1°C. However, when the rotational velocity increases to 20 rpm, the maximum temperature in the evaporator section rises to 25.1°C, while the temperature at the end of the condenser section drops to 20°C.

In Fig. 8(b), with the heat load increased to 110 W, the impact of rotational velocity becomes more pronounced. The temperature at the end of the condenser section decreases with increasing rotational velocity, showing a difference of 2.5°C between 0 rpm and 12 rpm. This temperature variation is attributed to centrifugal force generated during rotation, which hinders the return flow of the working fluid, causing the low-temperature liquid in the condenser section to flow slowly and thereby reducing the local temperature. When the rotational velocity increases to 20 rpm, the operating temperature of the evaporator section exceeds 50°C. For the purpose of safety, no tests were conducted at higher heat loads with 70mm condensation length.

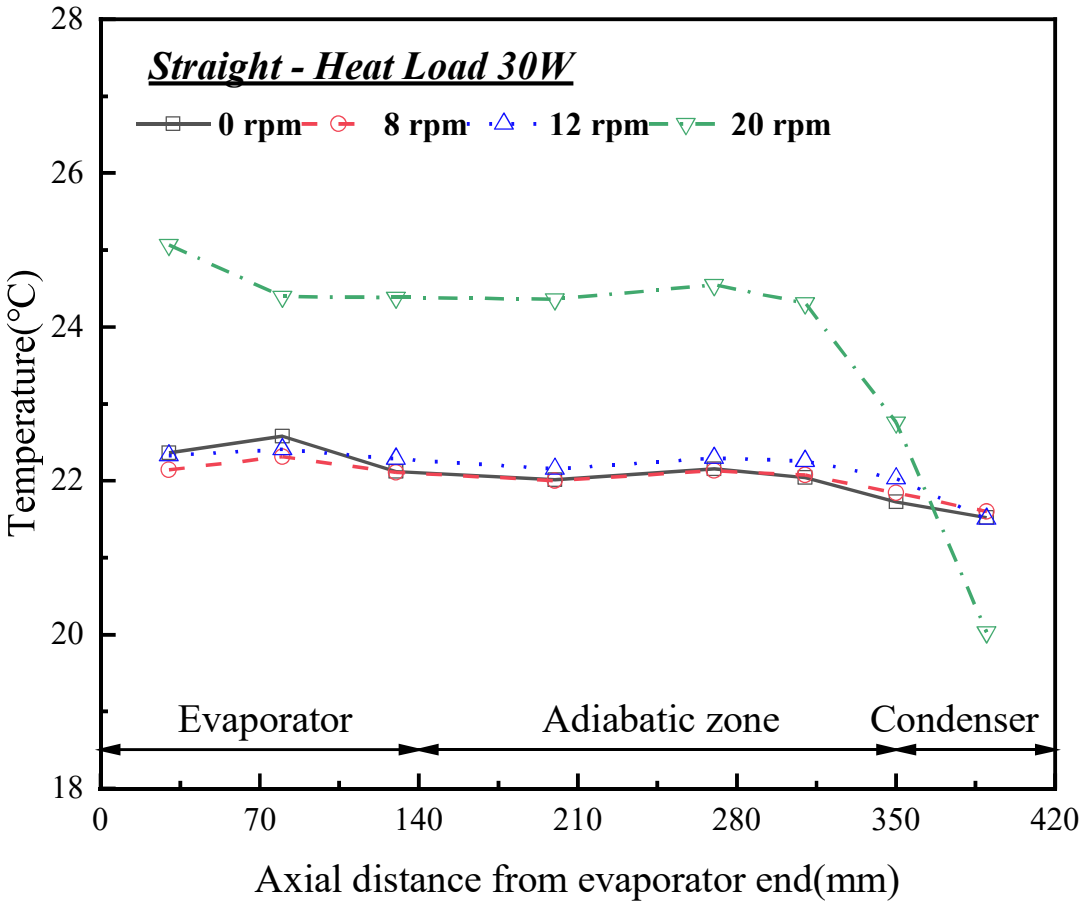

(a) 30 W

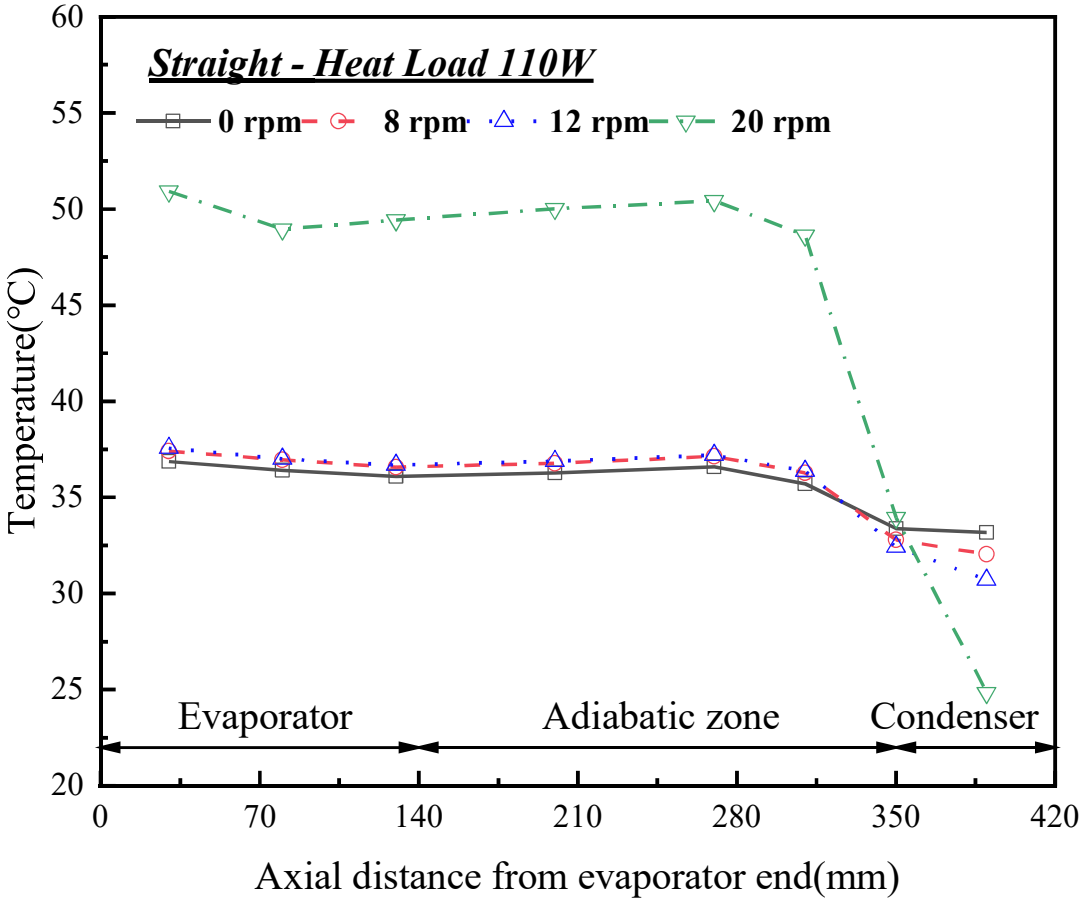

(b) 110 W

Fig. 8. Temperature Distribution versus Angular Velocities for 30 W and 110 W.

The observed changes in operating temperature can be explained by the following reasons. As the rotational angular velocity increases, the centrifugal force's resistive component at the end of the condenser section gradually increases until it exceeds the capillary force's driving capability. Consequently, the working fluid cannot return, leading to its accumulation at the condenser end. This effectively shortens the condensation length, reducing condensation efficiency. The insufficient return flow of the working fluid also lowers evaporation efficiency, resulting in an overall increase in the operating temperature of the heat pipe.

3.1.2. Effect of different heat loads

Fig. 9 shows the temperature variations at each measurement point for the straight grooved heat pipe with 70mm condensation length under different heat loads and rotational velocities, selecting static state and 20 rpm conditions. The overall operating temperature of each section of the heat pipe increases continuously with increasing power, with the evaporator section's temperature rising more than the condenser section's, resulting in an increasing temperature difference between the two.

In Fig. 9(a), it can be seen that under static state conditions, the overall operating temperature of the heat pipe increases with increasing power. The maximum temperature in the evaporator section rises from 22.3°C to 37.4°C, while the minimum temperature in the condenser section increases from 21.5°C to 31.1°C. This is because the increased heat transfer power requires a larger pressure gradient to drive more vapor flow and heat transfer, corresponding to a higher temperature gradient.

In Fig. 9(b), at high rotational velocities, centrifugal force causes the working fluid to accumulate in the condenser section, leading to the loss of heat transfer capability at the end, with the temperature remaining almost unchanged with increasing power. In contrast, the temperature in the evaporator section rises from 25°C to 51°C, while the condenser section's temperature only increases from 20°C to 24.8°C. Due to the shortened effective condensation length, the degree of temperature rise in the heat pipe is greater than at lower rotational velocities, causing the evaporator section to reach its maximum operating temperature at a lower heat load.

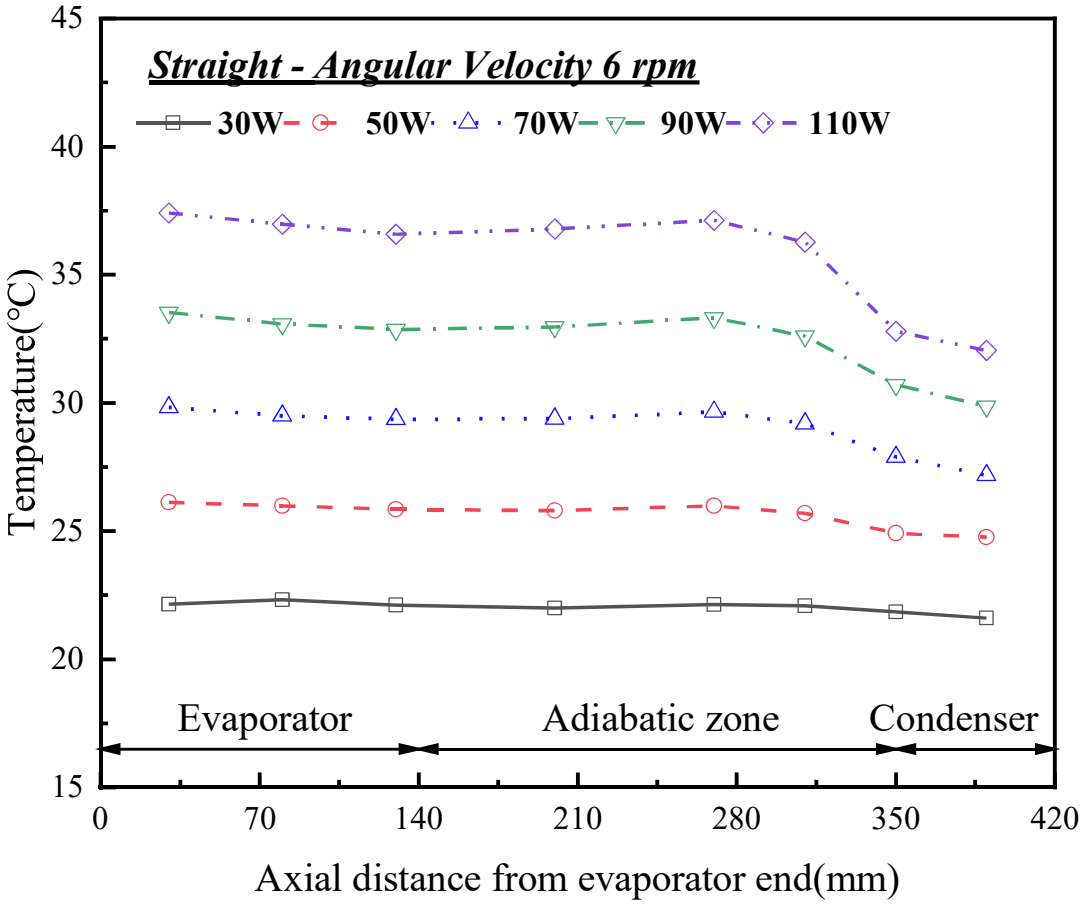

(a) 6 rpm

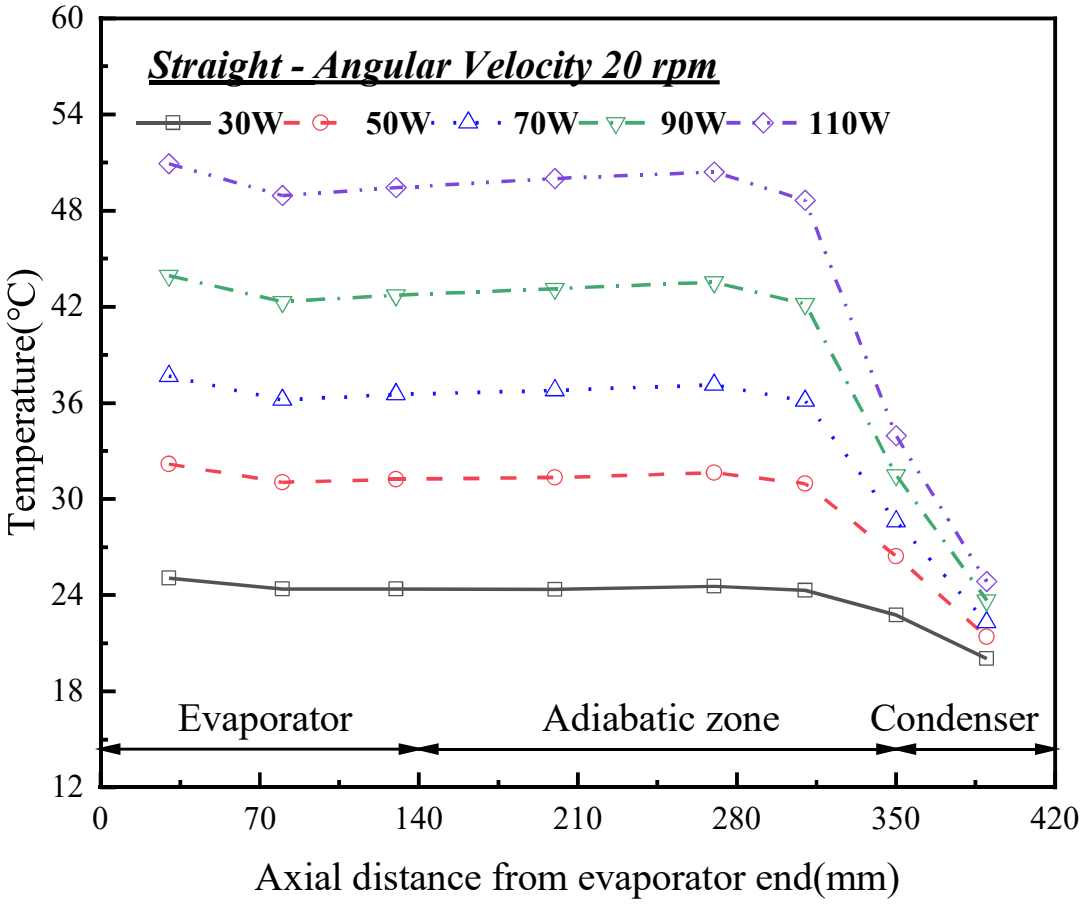

(b) 20 rpm

Fig. 9. Temperature Distribution versus Heat Loads for 8 rpm and 20 rpm.

3.1.3. Effect of different condensation lengths

Fig. 10 shows the temperature variations at each measurement point for the straight grooved heat pipe under different rotational velocities, condensation lengths, and heat loads. The increase in condensation length significantly enhances the cooling effect, resulting in lower operating temperatures under various rotational velocities and power conditions.

In Fig. 10(a), at a low rotational velocity of 8 rpm, increasing the condensation length reduces the heat transfer temperature difference from 3.7°C, 2.7°C, and 1.4°C to 1.6°C, 1.2°C, and 0.8°C, respectively, thereby improving the heat transfer performance of the heat pipe under low rotational velocity conditions.

However, in Fig. 10(b), it can be seen that although increasing the condensation length improves the cooling effect under high rotational velocities and reduces the excessively high operating temperatures, lowering the heat transfer temperature difference from 20.3°C, 15.3°C, and 10.7°C to 5.1°C, 3.0°C, and 2.7°C, it does not resolve the issue of working fluid accumulation in the condenser section. The problem of excessively large local temperature differences remains unaddressed.

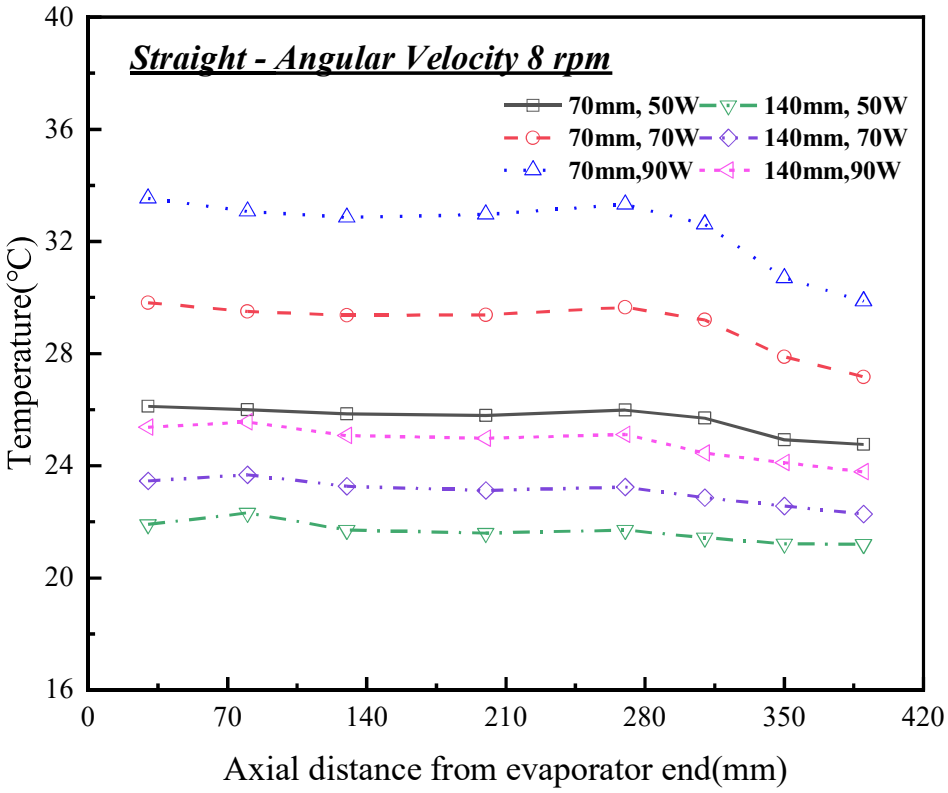

(a) 8 rpm

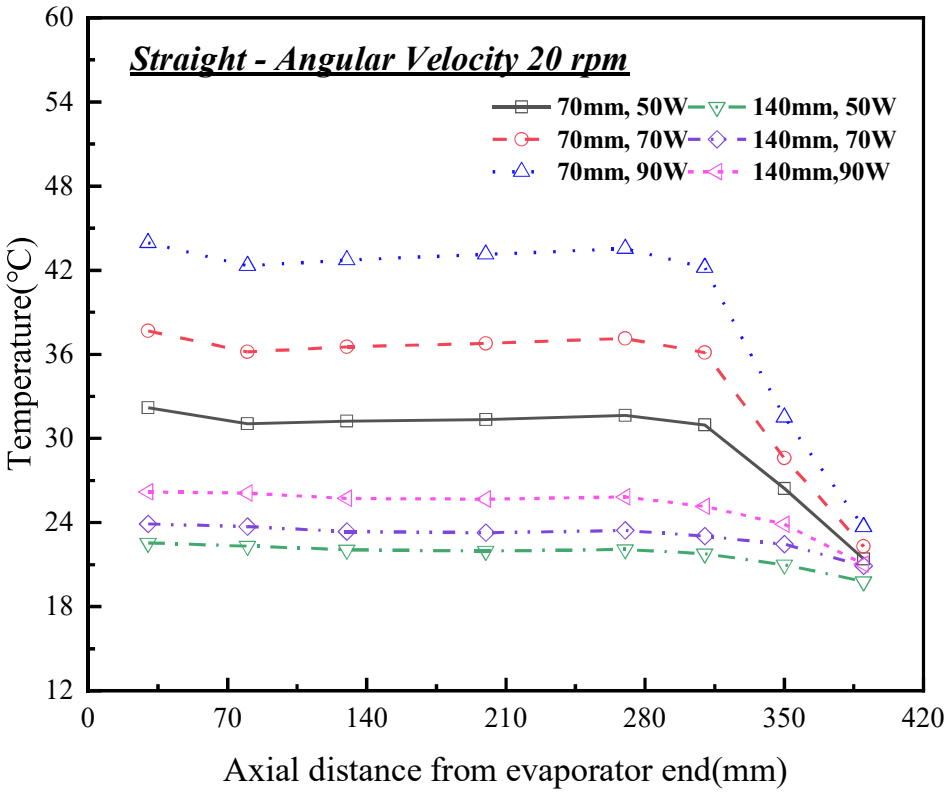

(b) 20 rpm

Fig. 10. Temperature Distribution versus Condensation Lengths for 8 rpm and 20 rpm.

In traditional straight grooved heat pipes, as the rotational angular velocity increases, liquid accumulates at the ends of the evaporator and condenser sections due to centrifugal force, leading to flow difficulties. The vapor generated in the evaporator section experiences less influence from centrifugal force and flows through the adiabatic section to condense in the condenser section. However, as the rotational velocity increases, the accumulation length in the condenser section continuously increases, reducing the effective condensation length until the condensation effect is entirely lost. During this process, the overall operating temperature difference of the heat pipe already exceeds the allowable range. Although the heat pipe still has some heat transfer capability, the effective heat transfer distance shortens, the overall operating temperature rises, and the heat pipe loses its overload resistance, ultimately failing due to the increased rotational angular velocity.

3.2. Steady-state operating characteristics of curve grooved heat pipes (AGHP2#)

Fig. 11 shows the variation in the acceleration components in the flow direction at different positions along the curved grooved heat pipe under rotational conditions. It can be observed that through the design of the variable curvature structure, the acceleration components in the adiabatic and condenser sections are maintained at relatively low positive values. This design prevents the issue of liquid accumulation in the condenser section during rotation. Meanwhile, the evaporator section retains the beneficial effect of acceleration on fluid return, which helps to enhance the heat transfer performance of the heat pipe under rotational conditions.

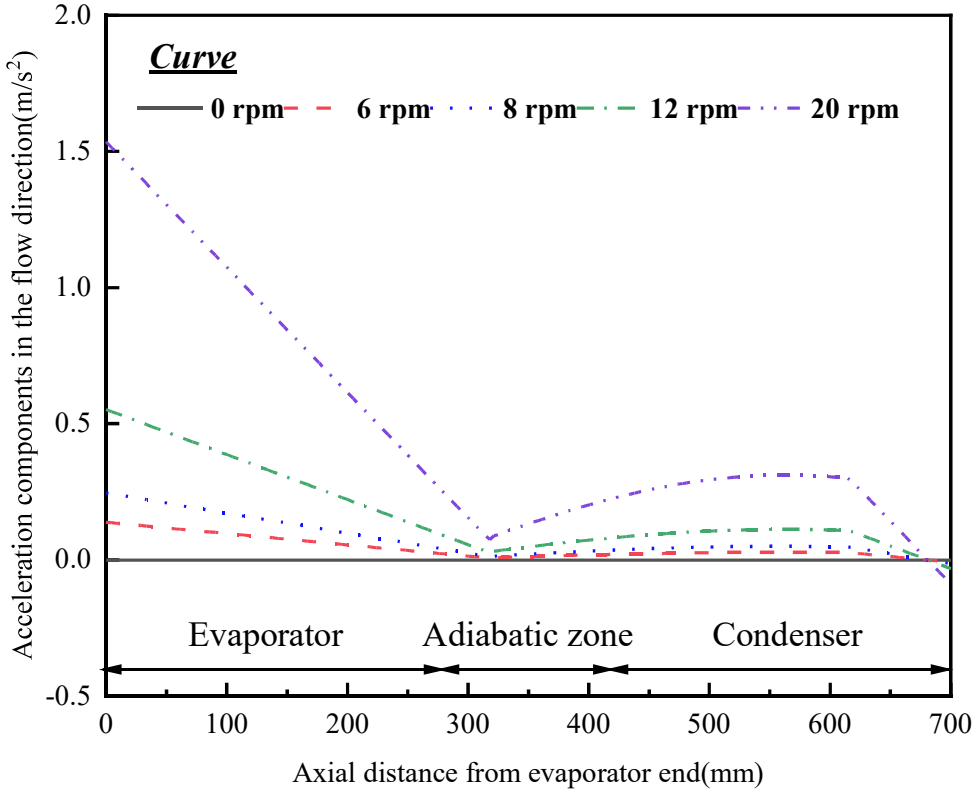

Fig. 11. Acceleration components in the flow direction of the curved grooved heat pipe

3.2.1. Effect of different rotational angular velocity

Fig. 12 shows the temperature variations at each measurement point for the curved grooved heat pipe under different rotational velocities and two different heat loads of 50 W and 210 W. With the assistance of centrifugal force aiding the return of the working fluid, the operating temperature decreases to varying degrees as the rotational velocity increases.

In Fig. 12(a), at 50 W, the rotational velocity of 20 rpm promotes the return flow of the working fluid so effectively that it causes liquid to accumulate at the evaporator end, changing the boiling mode from film boiling to pool boiling, which introduces a certain degree of superheat. Apart from this, as the rotational velocity increases, the maximum temperature in the evaporator section decreases from 20.5°C to 19.8°C, while the temperature at the end of the condenser section increases from 19.4°C to 19.7°C. This occurs since centrifugal force promotes the return of the working fluid, with the low-temperature fluid cooling the evaporator section, and as the condenser section space opens, the condensation of vapor raises the temperature of the condenser section, resulting in a more uniform overall temperature distribution.

In Fig. 12(b), with the power increased to 210 W, the temperature of the heat pipe decreases along the axial direction. As the rotational velocity increases, the temperature of the adiabatic section of the heat pipe decreases from 31.4°C to 30.4°C. This is because the increased rotational velocity improves the return flow of the working fluid, enhancing the condensation conditions and reducing the temperature difference with the heat sink, thereby lowering the operating temperature of the heat pipe. At 8 rpm, the temperature at the end of the evaporator section is more than 1.5°C higher than at other measurement points, with a difference of 5.3°C from the minimum temperature in the condenser section, indicating that the evaporator section may be experiencing dry-out and the heat pipe has reached its heat transfer limit at this rotational velocity.

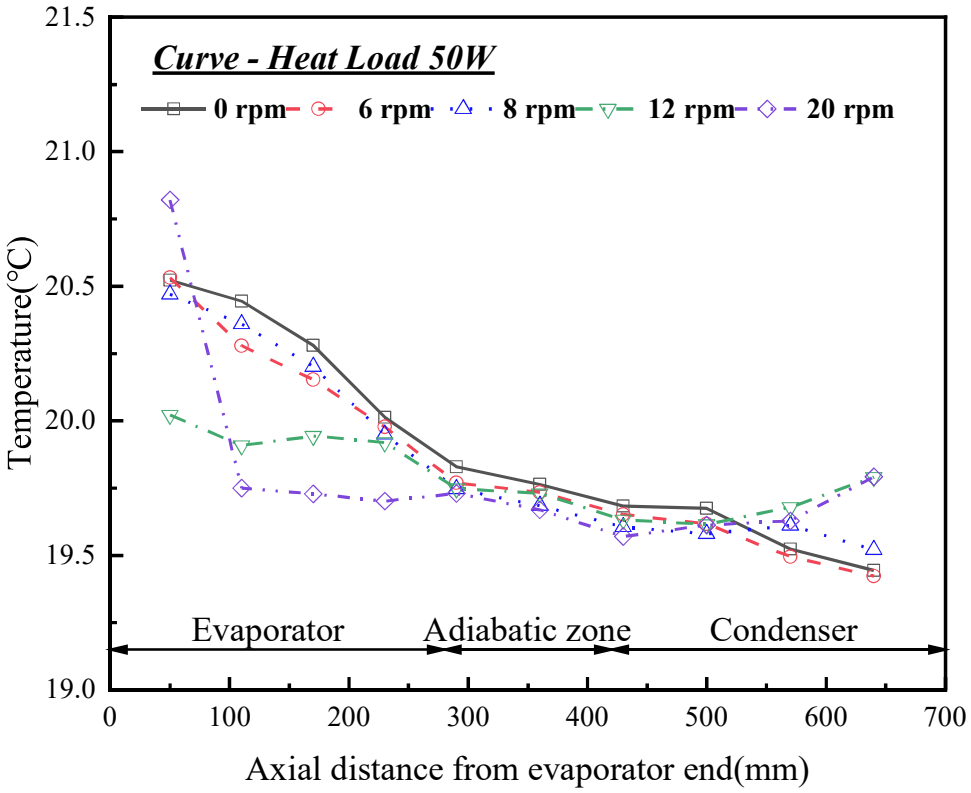

(a) 50 W

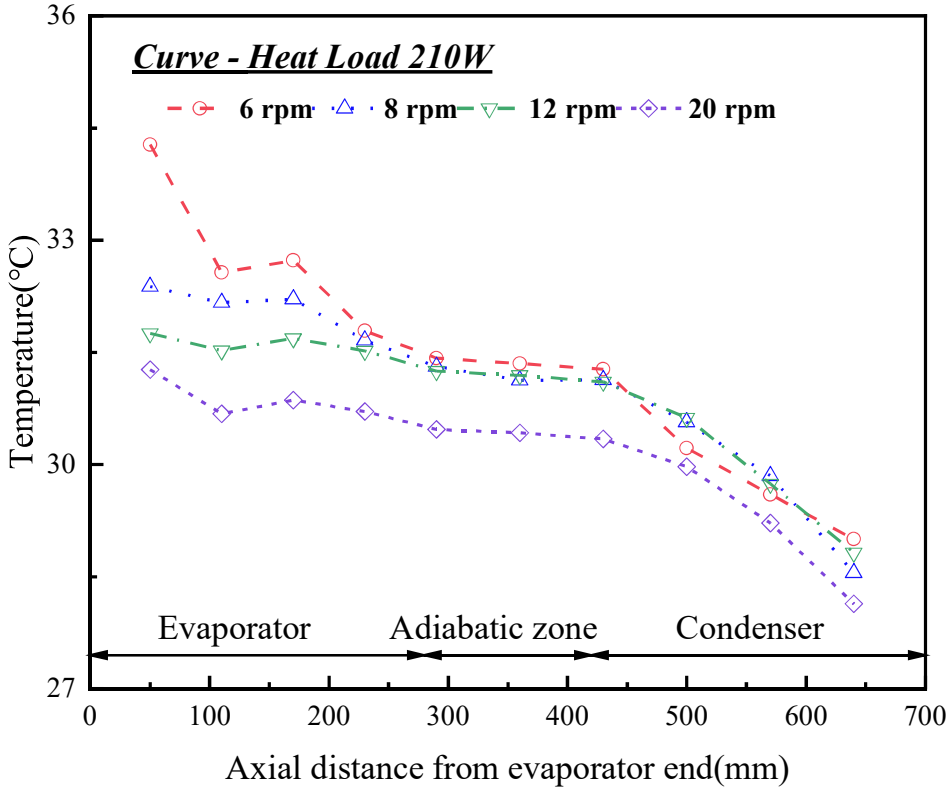

(b) 210 W

Fig. 12. Temperature Distribution versus Angular Velocities for 50 W and 210 W.

3.2.2. Effect of different heat loads

Fig. 13 shows the temperature variations at each measurement point for the curved grooved heat pipe under different rotational velocities and heat loads, with the conditions selected being static state, 12 rpm, and 20 rpm. The overall operating temperature of each section of the heat pipe increases continuously with increasing power, and the operational limit of the heat pipe is enhanced with increased rotational velocity.

In Fig. 13(a) at static state, the maximum temperature difference between the evaporator and condenser sections is 4.2°C at 150 W. When the power increases to 170 W, there is a significant temperature rise at the evaporator end, with the overall temperature difference reaching 5.4°C, indicating local dry-out in the evaporator section, thus reaching the heat transfer limit under these conditions.

In Fig. 13(b), with the application of a 12 rpm rotational velocity, centrifugal force leads to a more uniform temperature distribution in the heat pipe. As the heat transfer rate increases, a higher driving force is required to sustain more rapid vapor flow, resulting in an increased saturation vapor pressure difference between the evaporator and condenser sections, which in turn increases the temperature difference between the two ends. At this rotational velocity, there is no significant liquid accumulation at the evaporator end, and the overall operation is stable, with a temperature difference of 5.8°C at a 300 W load.

In Fig. 13(c), at a rotational velocity of 20 rpm, a higher temperature is observed at the evaporator end across different power levels. Unlike local dry-out, this temperature increase is due to centrifugal force promoting significant liquid return, creating liquid pits in the evaporator section and altering the boiling mode at the evaporator end. This requires superheating to maintain the boiling state, leading to a localized temperature difference at the evaporator end. This phenomenon does not affect the heat transfer limit of the AGHP but is a side effect of using centrifugal force to assist liquid return. As the heat transfer rate increases, the liquid level in the evaporator decreases, gradually eliminating this effect. However, at low power levels, this might cause the evaporator temperature to deviate from expected values, warranting attention in engineering applications.

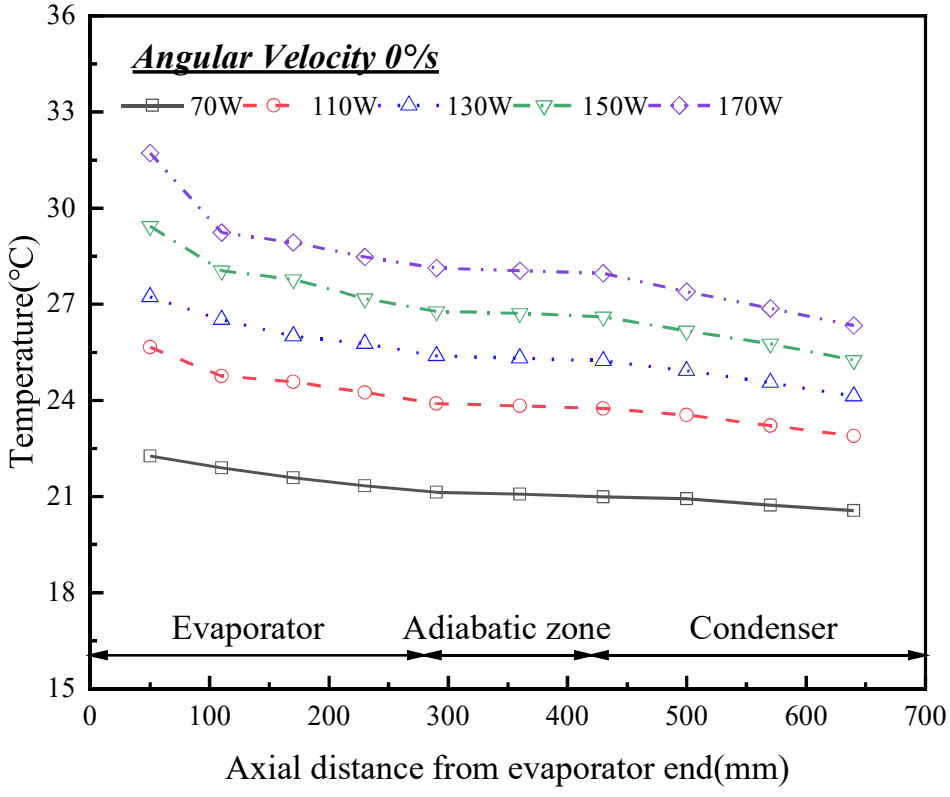

(a) 0 rpm

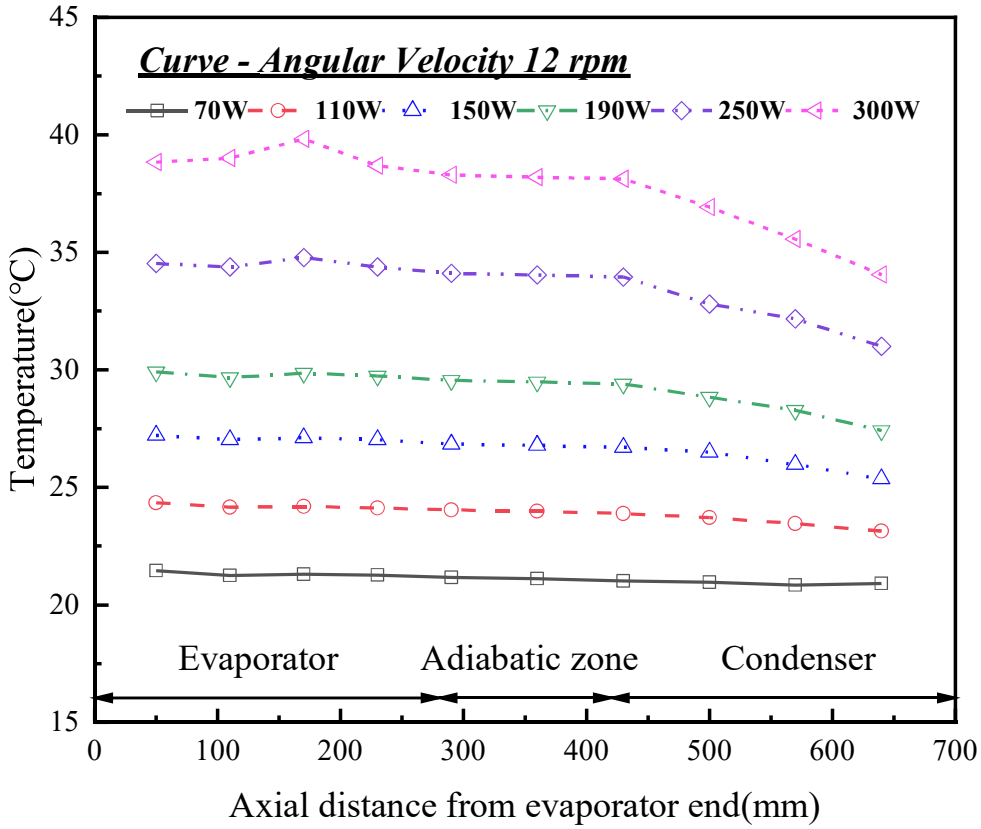

(b) 12 rpm

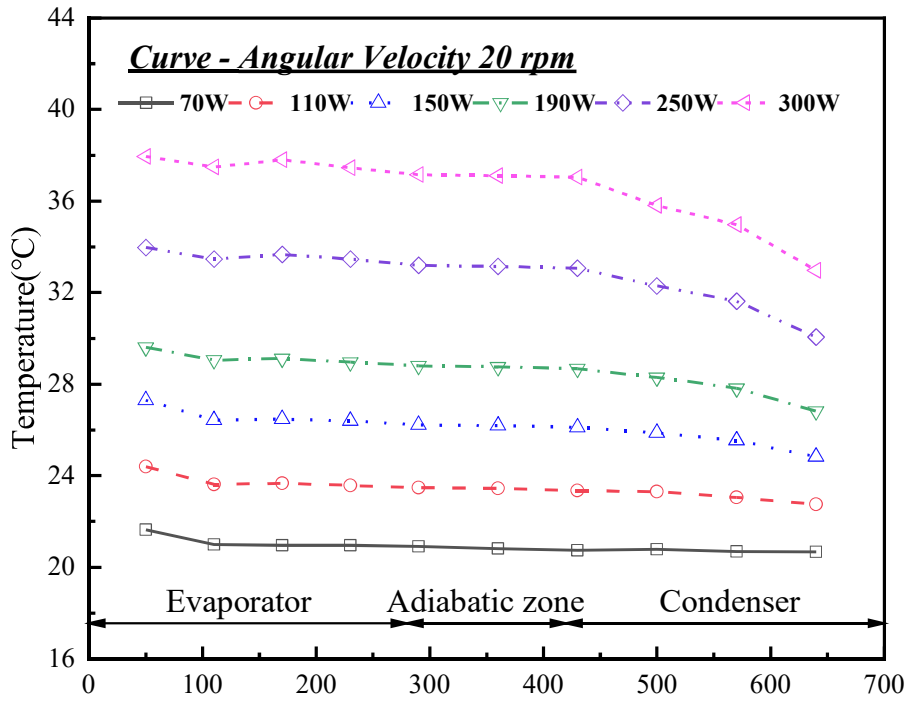

(c) 20 rpm

Fig. 13. Temperature Distribution versus Heat Loads for 0 rpm, 12 rpm and 20 rpm.

3.2.3. Effect of different loading methods

Fig. 14 shows the temperature variations at each measurement point for the curved grooved heat pipe under different loading methods and rotational velocities, with two different heat loads of 30 W and 90 W.

In Fig. 14(a), at 30 W and a low rotational velocity of 8 rpm, the maximum temperature in the evaporator section is 18.9°C, and the minimum temperature in the condenser section is 18.5°C. At a higher rotational velocity of 20 rpm, both loading methods show temperature increases at both ends of the heat pipe, with the evaporator section reaching 19.7°C and 19.8°C, and the condenser section reaching 19.2°C and 19.3°C, respectively.

In Fig. 14(b), at 90 W and a low rotational velocity of 8 rpm, the heat pipe exhibits a larger operating temperature difference, with the maximum temperature in the evaporator section being 23.6°C and the minimum temperature in the condenser section being 22.2°C. At the higher rotational velocity of 20 rpm, the end temperatures are higher, with the maximum temperature in the evaporator section being 23.3°C, while the temperature differences at other positions are smaller, and the minimum temperature in the condenser section is 22.1°C.

The final steady-state operating temperatures of the heat pipe are essentially the same regardless of the sequence in which thermal and mechanical loads are applied, demonstrating that the performance of the AGHP is not affected by the loading method.

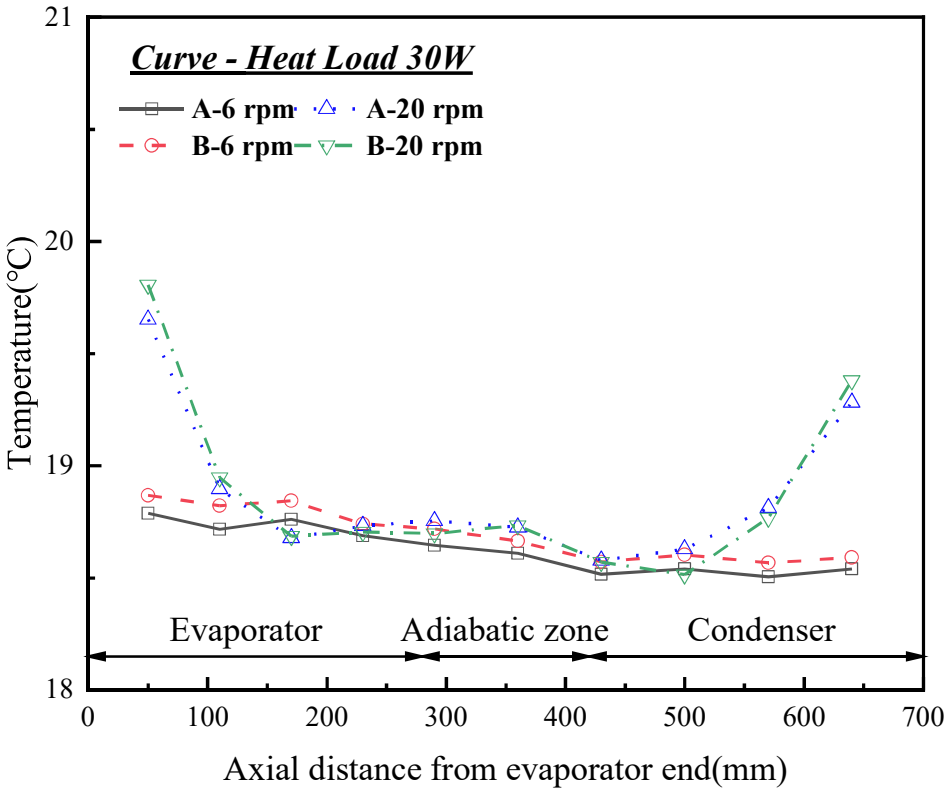

(a) 30 W

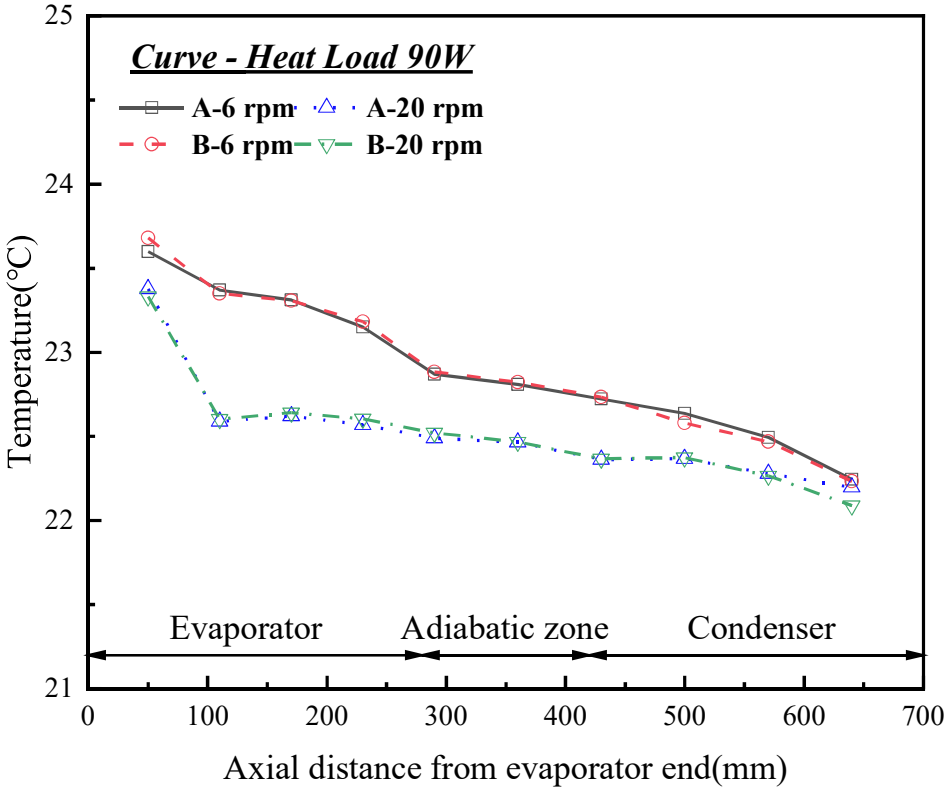

(b) 90 W

Fig. 14. Temperature Distribution versus Condensation Lengths for 30 W and 90 W.

The curved grooved adiabatic and condenser sections are minimally affected by centrifugal force, retaining only the beneficial impact of centrifugal force on liquid return in the evaporator section. This characteristic enhances the heat transfer limit of the heat pipe, which might otherwise be constrained by insufficient capillary action. Additionally, the assisted liquid return opens space for vapor condensation in the condenser section, strengthening the condensation heat transfer. This process raises the condenser section temperature while reducing the overall operating temperature difference. The simple internal structure of the grooved heat pipe allows it to maintain similar steady-state temperature distributions under different loading methods, demonstrating excellent load adaptability.

3.3. Comparison of AGHP1# and AGHP2#

3.3.1. Steady-state operating temperature

Fig. 15 compares the steady-state operating temperatures of the straight grooved heat pipe and the curved grooved heat pipe with a 140 mm condensation length under different heat loads. The curved grooved heat pipe exhibits better temperature uniformity in rotational states across various power levels compared to its static state, while the straight grooved heat pipe shows the opposite trend.

From Fig. 15(a), it can be seen that with a 140 mm condensation length at a low power of 30 W, the operating temperature of the straight grooved heat pipe, except for the end, is nearly the same as the static state. The curved grooved heat pipe, due to its design that utilizes centrifugal force to drive the return flow of the working fluid, shows the side effect of fluid accumulation at the evaporator end at low power.

In Fig. 15(b), when the thermal load increases to 150 W, the operating temperature and temperature difference of the straight grooved heat pipe with an extended condensation length remain high, reaching 10.8°C. In contrast, the temperatures at all points on the curved grooved heat pipe are lower than in the static state, with an operating temperature difference of only 2.5°C, indicating better performance than in the static state.

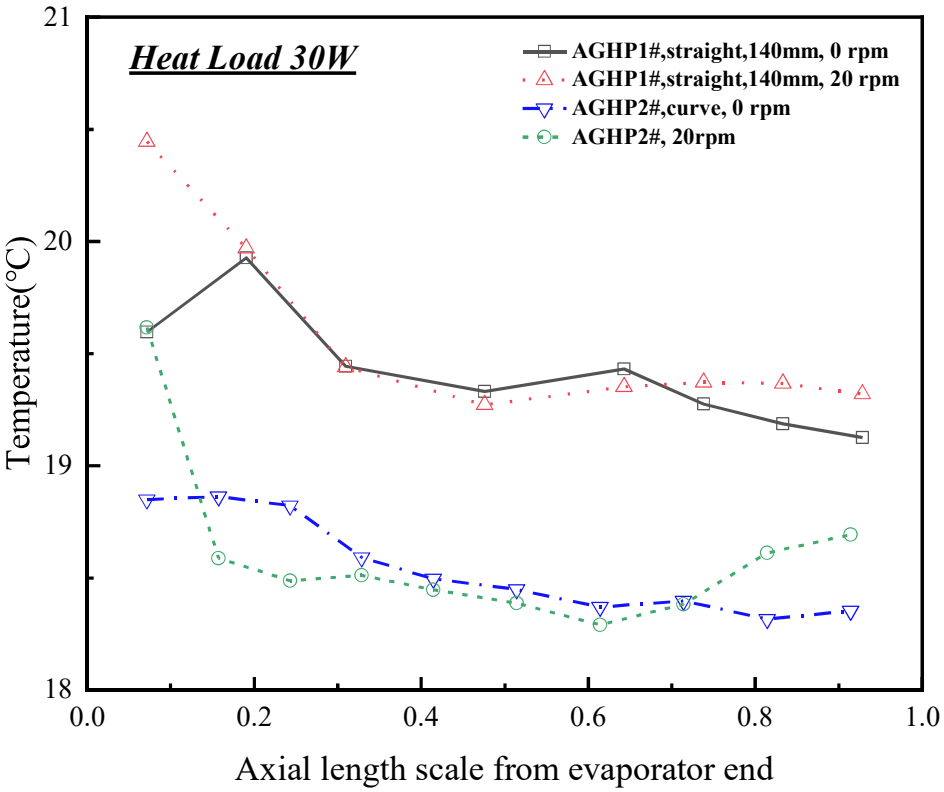

(a) 30 W

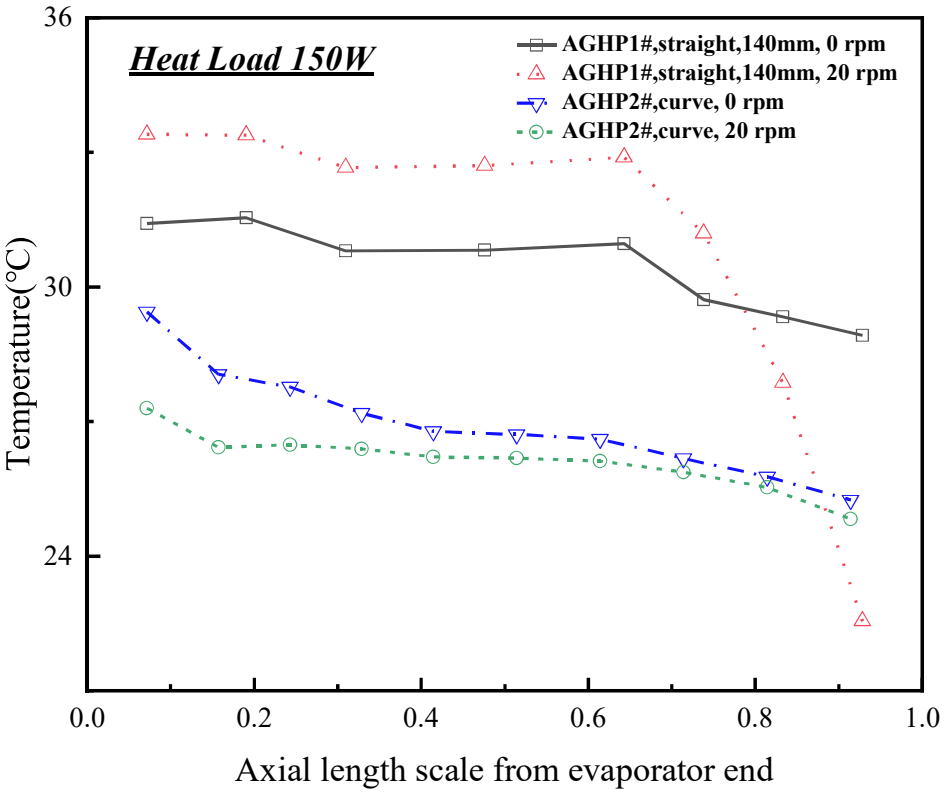

(b) 150 W

Fig. 15. Temperature Distribution for Different AGHPs for 30 W and 150 W.

3.3.2. Heat transfer limits and thermal resistance

Fig. 16 shows the variations in heat transfer limits with rotational angular velocity and the total thermal resistance with heat load for the straight grooved heat pipe and the curved grooved heat pipe, both with a condensation length of 140 mm.

In Fig. 16(a), due to the heat flux density limitation of the heating pad, specific values for the heat transfer limit of the straight grooved heat pipe at low rotational velocities could not be obtained. At 150 W, the heat transfer limit was not reached, but the analysis of the heat transfer temperature difference at the existing power levels suggests that the heat transfer limit decreases gradually with increasing rotational angular velocity, dropping to 90 W at 20 rpm. Conversely, as the rotational angular velocity increases, the return efficiency of the working fluid in the curved grooved heat pipe improves, and the heat transfer limit increases from 170 W in the static state to 300 W at 20 rpm.

In Fig. 16(b), for the straight grooved heat pipe at 20 rpm, as the heat load increases, the total thermal resistance initially decreases and then increases. Before reaching the heat transfer limit, the increased power enhances the evaporation and condensation heat transfer, leading to a decrease in thermal resistance. However, due to the influence of centrifugal force, the heat pipe quickly reaches its heat transfer limit, after which the internal heat transfer no longer changes significantly, and the excess heat is conducted through the metal wall, causing the thermal resistance to increase rapidly. Both heat pipes do not reach the heat transfer limit under static state conditions, resulting in smaller and more stable changes in thermal resistance.

For the curved grooved heat pipe, at low power, the working fluid accumulates at the evaporator end, forming liquid pits and entering a low-efficiency pool boiling state, resulting in higher thermal resistance. As the power increases, the evaporation mode shifts, leading to a rapid decrease in thermal resistance, which then stabilizes.

The curved grooved heat pipe, designed with centrifugal force-assisted liquid return, can reduce the operating temperature, increase the heat transfer limit, reduce the operating temperature difference, and decrease the thermal resistance. This design leverages centrifugal force to enhance performance during operation, resulting in superior performance under rotational conditions compared to static state conditions. However, it is important to be mindful of the side effect of liquid accumulation at the evaporator end under high rotational velocities and low power conditions to avoid adverse impacts during use.

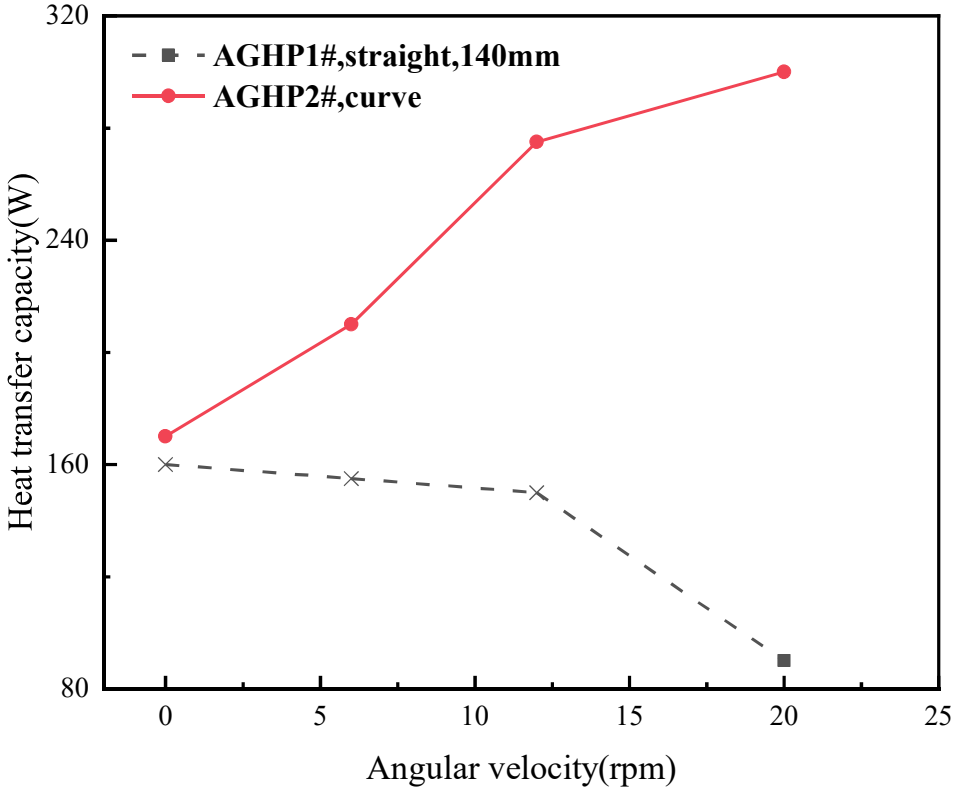

(a) Heat Transfer Limit

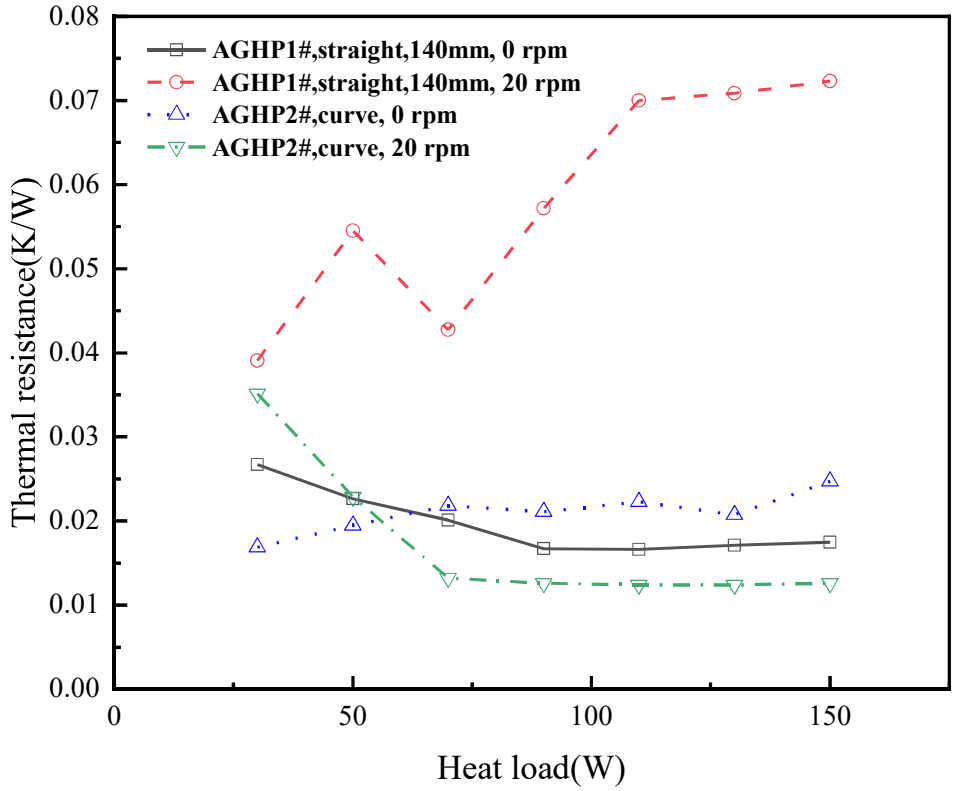

(b) Thermal Resistance

Fig. 16. Heat Transfer Limit and Thermal Resistance for Different AGHPs.

Existing research indicates that traditional straight grooved heat pipes tend to experience

liquid accumulation at the end of the condenser section under rotational conditions. This leads to a reduction in the effective condensation length, shortened heat transfer distance, and increased operating temperature. In contrast, grooved heat pipes with a variable curvature design demonstrate better performance, including lower operating temperatures, higher heat transfer limits, and reduced thermal resistance. In practical applications, a variable curvature design that gradually increases the rotation radius from the condenser to the evaporator section should be adopted to enhance fluid return and improve the performance of grooved heat pipes in rotational environments. If traditional straight grooved heat pipes are used, it is advisable to position the end of the condenser section closer to the rotational center to minimize performance degradation caused by liquid accumulation.

4. Conclusions

To gain a deeper understanding of the internal flow and heat transfer mechanisms in grooved heat pipes under rotational conditions and explore effective methods to enhance their performance, this study designed and fabricated a conventional straight grooved heat pipe and a specially designed curved grooved heat pipe. An experimental system was built to evaluate the performance of these heat pipes under rotational conditions, covering a range of rotational velocities (0-20 rpm), heat loads (30 W-300 W), and loading methods (Methods A and B). The study analyzed the effects of these factors on the steady-state operating characteristics of grooved heat pipes under rotational conditions, and the main conclusions are as follows:

(i) The straight grooved heat pipe could not function effectively under rotational conditions. Centrifugal force caused the working fluid to accumulate at both ends, reducing the effective heat transfer distance and increasing the overall operating temperature. For instance, at a rotational velocity of 20 rpm and a heat load of 110 W, the operating temperature difference exceeded 25°C, indicating that the heat pipe was not capable of functioning efficiently in rotational environments.

(ii) The curved grooved heat pipe performed well under rotational conditions. The design effectively reduced the impact of centrifugal force in the adiabatic and condenser sections, preventing liquid accumulation at the end of the condenser section.

(iii) The curved grooved heat pipe exhibited improved performance under rotational conditions, including lower operating temperatures, increased heat transfer limits, and reduced thermal resistance. The beneficial effects of centrifugal force in the evaporator section facilitated fluid return, enhancing the heat transfer limit while also increasing the available space in the condenser section and improving condensation efficiency. For example, at a rotational velocity of 20 rpm, the heat pipe successfully transferred over 300 W with an overall temperature difference not exceeding 5°C.

(iv) At high rotational speeds and low power levels, an obvious temperature increase was observed at the end of the evaporator section of the curved grooved heat pipe. Under these conditions, centrifugal force became the primary driver of fluid return, leading to excessive

fluid accumulation at the end of the evaporator section. This caused a shift in the evaporation site from the meniscus to the free liquid surface within the vapor chamber, resulting in increased thermal resistance and a certain degree of superheating. Therefore, it is important to avoid application scenarios with excessively high rotational speeds.

This study contributes to the understanding of fluid dynamics and heat transfer mechanisms in grooved heat pipes under rotational conditions. The variable curvature design explored in this research has shown potential in optimizing the performance of grooved heat pipes by enhancing fluid return and reducing the adverse effects of centrifugal force. This work fills a critical gap by systematically investigating the performance of grooved heat pipes across varying rotational speeds. These findings offer a basis for further exploration and could inform the design and application of heat pipes in rotating systems, suggesting new directions for future research.

Declaration of Interest Statement

The authors declare that they have no known competing financial interests or personal relationships that could have appeared to influence the work reported in this paper. No potential conflict of interest was reported by the authors.

Acknowledgements

The authors acknowledge the financial support provided by National Natural Science Foundation of China (Grant No. 12272027).

Data availability

Data will be made available on request.

References

[1] AS R C B, Xavier Jr A L. A unified satellite taxonomy proposal based on mass and size[J]. Advances in Aerospace Science and Technology, 2019, 4(04): 57.

[2] Li W J, Cheng D Y, Liu X G, et al. On-orbit service (OOS) of spacecraft: A review of engineering developments[J]. Progress in Aerospace Sciences, 2019, 108: 32-120.

[3] Lu Y, Shao Q, Yue H, et al. A review of the space environment effects on spacecraft in different orbits[J]. IEEE access, 2019, 7: 93473-93488.

[4] Zou A M, Kumar K D, de Ruiter A H J. Spacecraft attitude control using two control torques[J]. Information Sciences, 2017, 408: 23-40.

[5] Zanardi M C, Celestino C C, Borderes Motta G, et al. Analysis of analytical attitude propagators for spin-stabilized satellites[J]. Computational and Applied Mathematics, 2018, 37: 96-109.

[6] Janssens F L, van der Ha J C. Stability of spinning satellite under axial thrust and internal

mass motion[J]. Acta Astronautica, 2014, 94(1): 502-514.
[7] Kucharski D, Kirchner G, Lim H C, et al. Spin parameters of High Earth Orbiting satellites ETALON-1 and ETALON-2 determined from kHz Satellite Laser Ranging data[J]. Advances in Space Research, 2014, 54(11): 2309-2317.
[8] Zhou Y, Wei S, Zhang L, et al. Dynamic estimation of spin satellite from the single-station ISAR image sequence with the hidden Markov model[J]. IEEE Transactions on Aerospace and Electronic Systems, 2022, 58(5): 4626-4638.
[9] Ovchinnikov M Y, Penkov V I, Roldugin D S, et al. Single axis stabilization of a fast rotating satellite in the orbital frame using magnetorquers and a rotor[J]. Acta Astronautica, 2020, 173: 195-201.
[10] Yamada K, Nagano H. Development of a heat storage panel for micro/nano-satellites and demonstration in orbit[J]. Applied Thermal Engineering, 2015, 91: 894-900.
[11] Colgan N, Nellis G, Anderson M. Modelling and optimization of a forced convection heat exchanger for Mars waste heat rejection for power cycle and cryocooling applications[J]. Applied Thermal Engineering, 2024, 242: 122463.
[12] Interlenghi S F, de Medeiros J L, Ofélia de Queiroz F A. Novel air dehydration for life-support systems of manned-spacecraft: Supersonic separator technology[J]. Applied Thermal Engineering, 2022, 213: 118731.
[13] Butler A, Argyropoulos C. Mechanically tunable radiative cooling for adaptive thermal control[J]. Applied Thermal Engineering, 2022, 211: 118527.
[14] Taylor S, Boman N, Chao J, et al. Cryothermal vacuum measurement of thermochromic variable-emittance coatings with heating/cooling hysteresis for spacecraft thermal management[J]. Applied Thermal Engineering, 2021, 199: 117561.
[15] Xie B, Zhang W, Zhao J, et al. Design of VO2-based spacecraft smart radiator with low solar absorptance[J]. Applied Thermal Engineering, 2024, 236: 121751.
[16] Selvadurai S, Chandran A, Valentini D, et al. Passive thermal control design methods, analysis, comparison, and evaluation for micro and nanosatellites carrying infrared imager[J]. Applied Sciences, 2022, 12(6): 2858.
[17] Liu L, Zhang X, Liang H, et al. Deployable and self adaptive system of intelligent thermal control of a micro satellite[C]//2022 International Conference on Sensing, Measurement & Data Analytics in the era of Artificial Intelligence (ICSMD). IEEE, 2022: 1-6.
[18] Hardesty R, Parker K. Advanced thermal control for spacecraft applications[C]//Material Technologies and Applications to Optics, Structures, Components, and Sub-Systems II. SPIE, 2015, 9574: 75-90.
[19] Prajapati J C, Kachhia K B, Kosta S P. Fractional calculus approach to study temperature distribution within a spinning satellite[J]. Alexandria engineering journal, 2016, 55(3): 2345-2350.
[20] Ali A, Tong J, Ali H, et al. A detailed thermal and effective induced residual spin rate analysis for LEO small satellites[J]. IEEE Access, 2020, 8: 146196-146207.

[21] Mehta R C. Thermal Analysis of a Micro-Satellite in a Low Earth Orbit[J]. Journal of Aerospace Sciences and Technologies, 2019: 333-339.
[22] Zhou W, Xie P, Li Y, et al. Thermal performance of ultra-thin flattened heat pipes[J]. Applied Thermal Engineering, 2017, 117: 773-781.
[23] Naemsai T, Kammuang-lue N, Terdtoon P, et al. Numerical model of heat transfer characteristics for sintered-grooved wick heat pipes under non-uniform heat loads[J]. Applied Thermal Engineering, 2019, 148: 886-896.
[24] Alijani H, Çetin B, Akkuş Y, et al. Effect of design and operating parameters on the thermal performance of aluminum flat grooved heat pipes[J]. Applied Thermal Engineering, 2018, 132: 174-187.
[25] Tao H Z, Zhang H, Zhuang J, et al. Experimental study of heat transfer performance in a flattened AGHP[J]. Applied thermal engineering, 2008, 28(14-15): 1699-1710.
[26] Li Y, Chen S, He B, et al. Effects of vacuuming process parameters on the thermal performance of composite heat pipes[J]. Applied Thermal Engineering, 2016, 99: 32-41.
[27] Mehrali M, Sadeghinezhad E, Azizian R, et al. Effect of nitrogen-doped graphene nanofluid on the thermal performance of the grooved copper heat pipe[J]. Energy Conversion and Management, 2016, 118: 459-473.
[28] Li Y, Li N, Shao B, et al. Theoretical and experimental investigations on the supercritical startup of a cryogenic axially Ω-shaped grooved heat pipe[J]. Applied Thermal Engineering, 2023, 222: 119951.
[29] Anand A R. Effect of various parameters on heat transport capability of axially grooved heat pipes. Thermal Sci. Eng. Progress 24, 100890 (2021)[J]. 2021.
[30] Li Z. Design and preliminary experiments of a novel heat pipe using a spiral coil as capillary wick[J]. International Journal of Heat and Mass Transfer, 2018, 126: 1240-1251.
[31] Kundan A, Plawsky J L, Wayner Jr P C. Thermophysical characteristics of a wickless heat pipe in microgravity–constrained vapor bubble experiment[J]. International Journal of Heat and Mass Transfer, 2014, 78: 1105-1113.
[32] Wei A, Ren X, Lin S, et al. CFD analysis on flow and heat transfer mechanism of a microchannel Ω-shape heat pipe under zero gravity condition[J]. International Journal of Heat and Mass Transfer, 2020, 163: 120448.
[33] Zhang X, Zhang C, Chen Y. Role of latent heat storage in thermal performance of an axially grooved heat pipe[J]. International Journal of Heat and Mass Transfer, 2022, 198: 123415.
[34] Liu X, Chai Y, Li J, et al. Effect of evaporation and condensation section length ratio on thermal performance of aluminum flat plate heat pipe with different micro grooved wicks[J]. Applied Thermal Engineering, 2023, 233: 121115.
[35] Lv Y, Wang B, Gan Z, et al. Corner flow characteristics in a silicon-based ultra-thin flat-grooved heat pipe with double-end cooling[J]. International Journal of Thermal Sciences, 2024, 198: 108860.

[36] Tang H, Tang Y, Zhuang B, et al. Experimental investigation of the thermal performance of heat pipes with double-ended heating and middle-cooling[J]. Energy Conversion and Management, 2017, 148: 1332-1345.
[37] Anand A R. Investigations on effect of evaporator length on heat transport of axially grooved ammonia heat pipe[J]. Applied Thermal Engineering, 2019, 150: 1233-1242.
[38] Saygan S, Akkus Y, Dursunkaya Z, et al. Capillary boosting for enhanced heat pipe performance through bifurcation of grooves: Numerical assessment and experimental validation[J]. International Communications in Heat and Mass Transfer, 2022, 137: 106162.
[39] Ng V O, Hong X Y, Yu H, et al. Anomalously enhanced thermal performance of micro heat pipes coated with heterogeneous superwettable graphene nanostructures[J]. Applied Energy, 2022, 326: 119994.
[40] Chang W, Huang G, Luo K, et al. Ultra-efficient heat pipes enabled by nickel-graphene nanocomposite coatings: Concept and fundamentals[J]. Carbon, 2022, 191: 384-392.
[41] Cheng J, Wang G, Zhang Y, et al. Enhancement of capillary and thermal performance of grooved copper heat pipe by gradient wettability surface[J]. International Journal of Heat and Mass Transfer, 2017, 107: 586-591.
[42] Hamidnia M, Luo Y, Li Z, et al. Capillary and thermal performance enhancement of rectangular grooved micro heat pipe with micro pillars[J]. International Journal of Heat and Mass Transfer, 2020, 153: 119581.
[43] Li Y, Zhou W, He J, et al. Thermal performance of ultra-thin flattened heat pipes with composite wick structure[J]. Applied Thermal Engineering, 2016, 102: 487-499.
[44] Parand S, Ziaei-Rad M, Asghari S. Thermal performance analysis of a trapezoid-shape grooved heat pipe with different working fluids for zero gravity applications[J]. Thermal Science and Engineering Progress, 2023, 40: 101802.
[45] Sudhan A L S, Solomon A B, Sunder S. Heat transport limitations and performance enhancement of anodized grooved heat pipes charged with ammonia under gravity and anti-gravity condition[J]. Applied Thermal Engineering, 2022, 200: 117633.
[46] Zhang X, Wu S, Zhang C. Effect of inclination angles on thermal performance of a heat pipe with axially trapezoidal grooves[J]. Microgravity Science and Technology, 2022, 34(5): 102.
[47] Tang H, Lian L, Zhang J, et al. Heat transfer performance of cylindrical heat pipes with axially graded wick at anti-gravity orientations[J]. Applied Thermal Engineering, 2019, 163: 114413.
[48] Supowit J, Heflinger T, Stubblebine M, et al. Designer fluid performance and inclination angle effects in a flat grooved heat pipe[J]. Applied Thermal Engineering, 2016, 101: 770-777.
[49] Yu F, Yu C, Cao J, et al. Experimental analysis of the evaporation regimes of an axially grooved heat pipe at small tilt angles[J]. International Journal of Heat and Mass Transfer,

2018, 126: 334-341.
[50] Voigt I, Drossel W G. Experimental investigation of heat pipe performance under translational acceleration[J]. Heat and Mass Transfer, 2022, 58(2): 209-219.
[51] Xie Y, Pu W, Liu S, et al. Visualized experimental study on steady-state performance of a loop heat pipe under elevated acceleration fields[J]. Applied Thermal Engineering, 2024, 238: 121984.
[52] Han L, Xie Y, Zhu J, et al. Experimental and analytical study of dual compensation chamber loop heat pipe under acceleration force assisted condition[J]. International Journal of Heat and Mass Transfer, 2020, 153: 119615.
[53] Piasecka M, Maciejewska B, Piasecki A. Heat Transfer Calculations during Flow in Mini-Channels with Estimation of Temperature Uncertainty Measurements[J]. Energies, 2023, 16(3): 1222.